

Garnet porphyroblast timing and behaviour during fold evolution: implications from a 3-D geometric analysis of a hand-sample scale fold in a schist

N. E. TIMMS

Department of Earth Sciences, University of Liverpool, Liverpool, L69 3GP, UK (n.e.timms@liv.ac.uk)

ABSTRACT Detailed 3-D analysis of inclusion trails in garnet porphyroblasts and matrix foliations preserved around a hand-sample scale, tight, upright fold has revealed a complex deformation history. The fold, dominated by interlayered quartz–mica schist and quartz-rich veins, preserves a crenulation cleavage that has a synthetic bulk shear sense to that of the macroscopic fold and transects the axis in mica-rich layers. Garnet porphyroblasts with asymmetric inclusion trails occur on both limbs of the fold and display two stages of growth shown by textural discontinuities. Garnet porphyroblast cores and rims pre-date the macroscopic fold and preserve successive foliation inflection/intersection axes (FIAs), which have the same trend but opposing plunges on each limb of the fold, and trend NNE–SSW and NE–SW, respectively. The FIAs are oblique to the main fold, which plunges gently to the WSW. Inclusion trail surfaces in the cores of idioblastic porphyroblasts within mica-rich layers define an apparent fold with an axis oblique to the macroscopic fold axis by 32°, whereas equivalent surfaces in tabular garnet adjacent to quartz-rich layers define a tighter apparent fold with an axis oblique to the main fold axis by 17°. This potentially could be explained by garnet porphyroblasts that grew over a pre-existing gentle fold and did not rotate during fold formation, but is more easily explained by rotation of the porphyroblasts during folding. Tabular porphyroblasts adjacent to quartz-rich layers rotated more relative to the fold axis than those within mica-rich layers due to less effective deformation partitioning around the porphyroblasts and through quartz-rich layers. This work highlights the importance of 3-D geometry and relative timing relationships in studies of inclusion trails in porphyroblasts and microstructures in the matrix.

Key words: deformation partitioning; Inclusion trails; rotation axis.

INTRODUCTION

Porphyroblast growth and behaviour during deformation, including folding, has attracted much attention and often heated discussion over the past two decades, and are currently very interesting topics for analysis by new quantitative microstructural approaches (Bell *et al.*, 1992; Passchier *et al.*, 1992; Forde & Bell, 1993; Mancktelow & Visser, 1993; Williams & Jiang, 1999; Stallard & Hickey, 2001; Kraus & Williams, 2001). Previous studies of porphyroblast inclusion trail geometry provide substantial evidence to strongly suggest porphyroblast nucleation and growth is directly related to development of crenulation cleavages (Bell, 1985; Bell *et al.*, 1986; Bell & Hayward, 1991; Williams, 1994; Spiess & Bell, 1996; Spear & Daniel, 2001). However, porphyroblast behaviour during growth and deformation is disputed and two different models exist that shall be referred to as the rotation model and the non-rotation model. Porphyroblast rotation vs. non-rotation depends on how matrix deformation is modelled (Fig. 1). The rotation model, primarily based on flow theory, considers rigid particles embedded in a flowing

homogeneous matrix (Jeffrey, 1922; Ghosh & Ramberg, 1976; Jęzek *et al.*, 1994). Shear coupling between rigid porphyroblasts and the actively flowing matrix causes porphyroblasts to rotate (Williams & Schoneveld, 1981; Passchier *et al.*, 1992; Williams & Jiang, 1999). Generally, rigid objects with higher aspect ratios and higher angles to the bulk flow are expected to rotate for two-dimensional homogeneous noncoaxial flow (Pennachioni *et al.*, 2001; Piazzolo *et al.*, 2002). Rigid particle rotation can be thought of in terms of ‘shear-induced vorticity’ and ‘spin’ induced rotation (Means *et al.*, 1980; Passchier & Trouw, 1996; Fig. 1). The non-rotation model incorporates deformation partitioning into zones of dominantly progressive shear, shortening and little or no strain (Bell, 1981). In this model, porphyroblast growth occurs early in crenulation development within zones of little or no strain. Growth ceases when zones of progressive shear impinge on their margins as the crenulation cleavage develops (Bell, 1985; Bell *et al.*, 1986; Bell & Johnson, 1992). Cessation of porphyroblast growth is followed by intensification of the new foliation against its margin. Porphyroblast rotation is inhibited due to the lack of shear coupling with the matrix. Growth

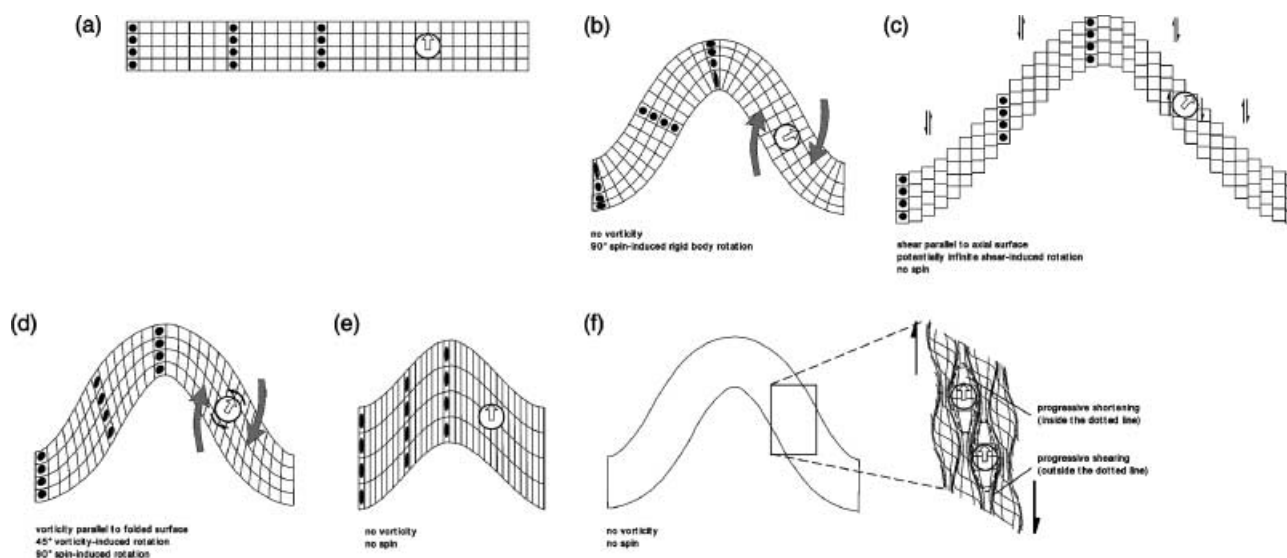


Fig. 1. Contrasting effects of five end-member fold mechanisms on porphyroblast rotation (adapted from Stallard, 1999). 'Vorticity' (specifically shear-induced vorticity) is the average angular velocity of lines relative to the instantaneous stretching axis, whereas 'spin' is the angular velocity of the stretching axes (e.g. bodily rotation of the fold limbs) relative to some external reference frame (see Passchier & Trouw, 1996). (a) Pre-deformation grid with strain markers (black circles) and porphyroblast. (b) In tangential longitudinal strain, folds develop by spin of the fold limbs (grey arrows) and strain is coaxially accumulated within a folded layer. Porphyroblasts are rotated an amount equivalent to the spin of the fold limbs. (c) During slip folding, shear is accommodated parallel to the axial plane of the fold and potentially produces unlimited rotation of porphyroblasts as limb rotation approaches 90° . (d) In flexural flow, layers are folded by simple shear parallel to the folded surface. This results in vorticity-induced rotation of porphyroblasts (black arrows) that is opposite to the spin of the fold limbs (grey arrows). In most cases, this results in net rotation consistent with, but of a lesser amount than the spin of the fold limbs. (e) Pure shear folding involves homogeneous coaxial shortening with no rotation of porphyroblasts relative to geographic co-ordinates. (f) In progressive bulk inhomogeneous shortening porphyroblasts occupy zones of 'little or no strain'. Strain is partitioned around these into zones of progressive shearing and progressive shortening. No shear coupling between porphyroblasts and matrix is established and no rotation occurs relative to geographic co-ordinates. All five fold models assume plane strain (i.e. no elongation in the third dimension).

over the 'new' foliation does not occur until early during a subsequent deformation event (Bell & Hayward, 1991).

Bell & Forde (1995) concluded that three-dimensional criteria to test rotation vs. non-rotation should be used, such as spiral axes of inclusion trails or foliation inflection/intersection axes preserved in porphyroblasts (FIAs). The timing of porphyroblast growth relative to the fold evolution is crucial for interpretation of porphyroblast behaviour and fold mechanism evolution. In order to understand porphyroblast behaviour, it is important to characterise processes and mechanisms operating at a grain/porphyroblast scale. It is therefore necessary to use the type and distribution of microstructures to infer how porphyroblasts have behaved when, where, and at what scale. Previous studies regarding the relationship between folding and porphyroblast behaviour have been limited by being either two-dimensional (e.g. Vissers & Mancktelow, 1992; Forde & Bell, 1995; Mancktelow & Visser, 1993), completely theoretical (e.g. Williams & Jiang, 1999; Jiang, 2001), or of regional-scale folds where there exists uncertainty in spatial and temporal correlation of foliations and porphyroblasts (e.g. Busa & Gray, 1992; Bell & Hickey, 1997; Bell *et al.*, 1997; Hickey & Bell, 1999, 2001; Stallard & Hickey, 2001; Bell & Chen, 2002).

This study evaluates shape and timing on porphyroblast behaviour by documenting in detail the 3-D geometry of microstructures in porphyroblasts and in the matrix of a hand-sample scale fold. Quantification of foliations preserved within porphyroblasts and the matrix as well as determination of FIAs and matrix intersection lineations for different parts of the fold has provided an integrated understanding of porphyroblast growth and behaviour with matrix deformation in three-dimensions during folding.

GEOLOGICAL SETTING

The area from where this sample was taken is dominated by regionally metamorphosed Ordovician to Silurian sedimentary rocks forming part of the 'New Hampshire Sequence', which form a NE-SW trending portion of the Appalachians (Billings, 1935, 1937). The large spatially orientated sample that forms the basis of this study (NT191, Timms, 2002) came from the east end of Cottonstone Mountain in the Orford area, west-central New Hampshire, and its exact location is at $72^\circ 04' 43''$ -W, $43^\circ 55' 03''$ -N (IMG 3453 6665). Conventional geothermobarometry of garnet-bearing metapelites in the area provide pressure and temperature estimates of between 4.7 and 6.6 kbar and 500 to 580°C (Spear & Rumble, 1986; Florence *et al.*, 1993).

The fold is of a relatively uncommon orientation for mesoscale folds in the area, lies oblique to the nappe stage and a dome stage folds that have been previously recognised in the area by Rumble (1969), and late in the complex deformation history of Timms (2002). It is structurally located on the east limb of the NE–SW trending Sunday Mountain Synclinorium, which Rumble (1969) considered was a consequence of the dome stage of folding. Deformation and metamorphism were synchronous and are assumed to coincide with the Devonian Acadian Orogenesis (Rumble, 1969; Bradley, 1983; Sutter *et al.*, 1985; Timms, 2002).

METHODS

The microstructural analysis consisted of measurements made from arrays of differently oriented thin sections cut every 10° around a compass from each limb of the fold. A total of over 60 thin sections were cut from the fold. These thin sections examined the equivalent layers from each limb of the fold allowing direct comparison of microstructures, and minimising any effects bulk composition variation may have had on deformation partitioning. Consequently, only a few thin sections were cut from the narrow hinge region due to space issues.

For the purposes of this study, foliation nomenclature is descriptive and specific to this fold sample only. This avoids correlation conflicts with established regional foliation (S) or deformation (D) hierarchies. Generally, foliations in the matrix, or external foliations, have the prefix of 'Se', and those preserved as inclusion trails in porphyroblasts, or internal foliations, have the prefix 'Si'.

Characterising foliations preserved in the matrix and within porphyroblasts

All linear measurements of a given plane should lie within that plane when plotted on a stereonet regardless of the orientation of the measurement. Therefore, foliations have been characterised by measuring pitches of their trace on a fanned array of vertical thin sections cut at 10° intervals around the compass and a horizontal oriented thin section, using a petrographic microscope. A minimum of 10 data was collected from each thin section for each Se, with considerably more in most cases. Measurements were made from all porphyroblasts in each thin section to characterise Si. This is important for thorough assessment of porphyroblast rotation (or lack thereof), as discussed below. A total of 1216 matrix pitch measurements and 1379 inclusion trail pitch measurements from the 62 thin sections have been used in this study. Pitch measurements were plotted on equal area stereonets and best-fit great circles with statistical constraints were calculated (Mancktelow, 1992). Best-fit pole constraint contours and standard deviation statistics give an indication of the real angular deviation of the pitch data from single orientation planar surfaces. These data have been used to assess the orientation and surface planarity of each type of microstructure on either side of the fold. All microstructures (Se & Si) described herein have been measured in this way to allow direct comparison. Analytical angular errors are relatively small and include initial sample orientation ($< \pm 3^\circ$), sample re-orientation in the laboratory ($< \pm 3^\circ$), thin section preparation ($\pm 1^\circ$) and pitch measurements using a petrographic microscope (in the order of 1°). However, sample orientation and re-orientation errors can be disregarded for relative comparison of data giving a maximum relative angular error of $\pm 2^\circ$.

Determining FIAs and matrix intersection lineations

Two independent methods have been used to determine FIAs for populations of porphyroblasts. The first, known as the 'plane intersection method', involves calculating the intersection of planes

estimated from pitch measurements as mentioned above (Stallard, 1999; Timms, 2002; Fig. 2). This has been applied to determine FIAs where inclusion tails are continuous but sharply inflected into different parts of the porphyroblast or into the matrix. Where this occurs, the inclusion trail and the trace of maximum inflection were measured (Fig. 2). Where inclusion trails are truncated and cannot be texturally related to crenulations this technique has not been applied. Here, the FIA trend, plunge and range have been calculated by the second technique. This method, known herein as the 'asymmetry switch method', involves observing the asymmetry switch from arrays of differently oriented thin sections (Bell *et al.*, 1995, 1997). If asymmetric microstructures (such as inclusion trails) are observed on a fanned array of oriented thin sections maintaining the same viewing direction, then a flip in asymmetry occurs where the axis is crossed. This is the foliation inflection/intersection axis, or 'FIA'. The FIA trend is calculated by observations made on the same oriented vertical thin sections as used in the 'plane intersection method' viewed in a consistent direction around the compass (Fig. 2). The FIA plunge is determined by similar observations made on an array of differently dipping thin sections containing the strike perpendicular to the FIA trend. FIAs obtained in this way are an average of all the porphyroblasts used. If the FIAs for individual porphyroblasts are not parallel, or the inclusion trail curvature is not cylindrical, then both asymmetries may be observed in different porphyroblasts in the same thin section. Therefore, the angular range has been calculated for FIAs where this occurs (Fig. 2).

Intersection lineations from crenulations in the matrix have been determined by the asymmetry switch method only. This is because the variable development of crenulations along hinges and between hinges makes it difficult and inappropriate to determine crenulated surfaces from measured pitches. Therefore, only matrix crenulation axial planes, which are commonly considerably straighter, have been determined from pitches in thin sections. Matrix intersection lineations and FIAs are similar microstructures and have been measured and plotted in similar way to allow direct comparison.

DATA DESCRIPTION/RESULTS

Description of the fold

The sample (NT191) contains a tight, asymmetric antiform with a relatively narrow hinge zone and limbs with low curvature (Figs 3 & 4). The antiform in NT191 is one of a series of small fold hinges bound on either side by asymmetric long limbs. The fold is defined by medium to dark grey mica-rich metapelitic schist heterogeneously interlayered (on a centimetre scale) with quartz-rich layers. The mica-rich layers dominate and alternate with variable thickness quartz-rich layers which commonly terminate abruptly, bifurcate and grade laterally into mixed quartz-mica layers (mixed layers). The axial plane strikes ENE–WSW and dips 70° SSE. The axial plunge of the hinge is variable between *c.* 10 to 30° to the WSW over 50 cm (outcrop scale). Mica-rich and quartz-rich layer geometries have been classified individually by conventional dip isogon method and tangential thickness methods (Ramsay, 1967; pp. 359–362; Fig. 5, this paper). Generally, quartz-rich layers do not have a substantially different geometry to that of the mica-rich layers and approximate a class two similar fold of Ramsay (1967; Fig. 5). The folded compositional domains (Se₀) have a strong parallel foliation (Se₁). A well-developed crenulation cleavage Se_{AP} deforms the

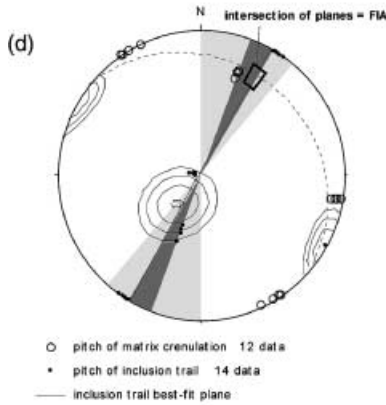
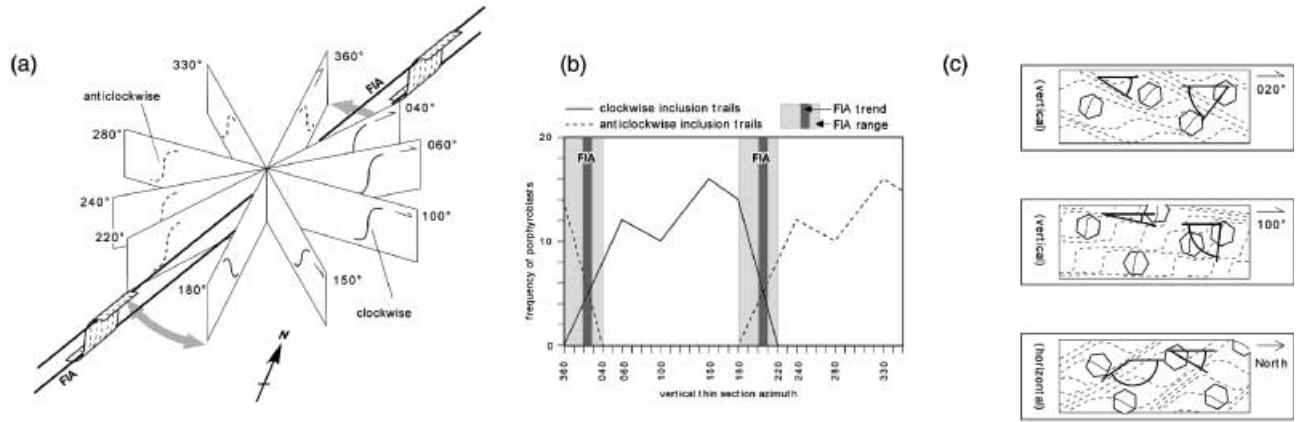


Fig. 2. Two different techniques for determining FIAs. The example given is for simple sigmoid inclusion trails in garnet porphyroblasts. (a) The asymmetry switch method (after Bell *et al.*, 1995). In this example, the axial trend of a simple sigmoid inclusion trail is between 180° and 220° (alternatively 360–040°). The grey arrows represent the angular range to within which the FIA has been determined. (b) An example of how FIAs and FIA ranges are determined graphically. The frequency of clockwise vs. anticlockwise asymmetries is plotted for each thin section azimuth. The FIA trend (dark grey) corresponds to the crossover, or switch in asymmetries. The range (light grey) is defined by the interval in which both asymmetries are present. (c) The plane intersection method of FIA determination. The pitches measured of the straight part of inclusion trails are measured on the oriented vertical thin sections, and the strike is measured on the horizontal section. In the example given, the inclusion trails are continuous with- and can be directly related to a matrix crenulation. Therefore, pitch or the strike of the matrix crenulation axial trace is also measured. (d) The pitches and strikes measured in (c) are plotted on an equal-area lower-hemisphere stereonet, and best-fit planes and constraint contours are calculated. The FIA is the intersection of the two planes. The trend determined from the method shown in (a) and (b) is indicated by the grey areas.

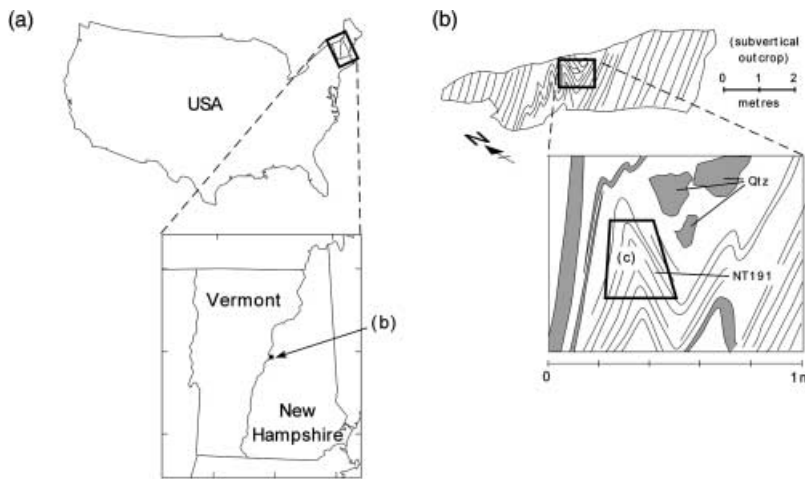


Fig. 3. (a) Geographic location of sample NT191. (b) Field sketches of the outcrop from which NT191 was taken.

dominant matrix foliation Se_1 in mica-rich and mixed layers with a synthetic sense of shear to the bulk fold geometry. Field measurements indicate that Se_{AP} transects the fold axis within the sampled volume, and is not parallel to the axial plane away from the fold hinge and sampled volume of rock (Fig. 4). This may be evidence of reactivation of the axial planar cleavage (Se_{AP}) away from the fold hinges, and the propensity for extra complexity in structural history (therefore geometry) within the fold is acknowledged. The matrix

of mica-rich layers is dominated by fine muscovite, quartz and very fine opaques (graphite?). It also contains abundant ilmenite grains, and minor amounts of chlorite, plagioclase and tourmaline. Quartz-rich layers comprise over 90% quartz, with chlorite and biotite forming the remaining interstitial grains. Quartz grain size in these domains is variable and commonly coarse, especially in the thicker quartz-rich layers. Both limbs of the fold contain abundant porphyroblasts of garnet, biotite (commonly partially pseudomorphed by

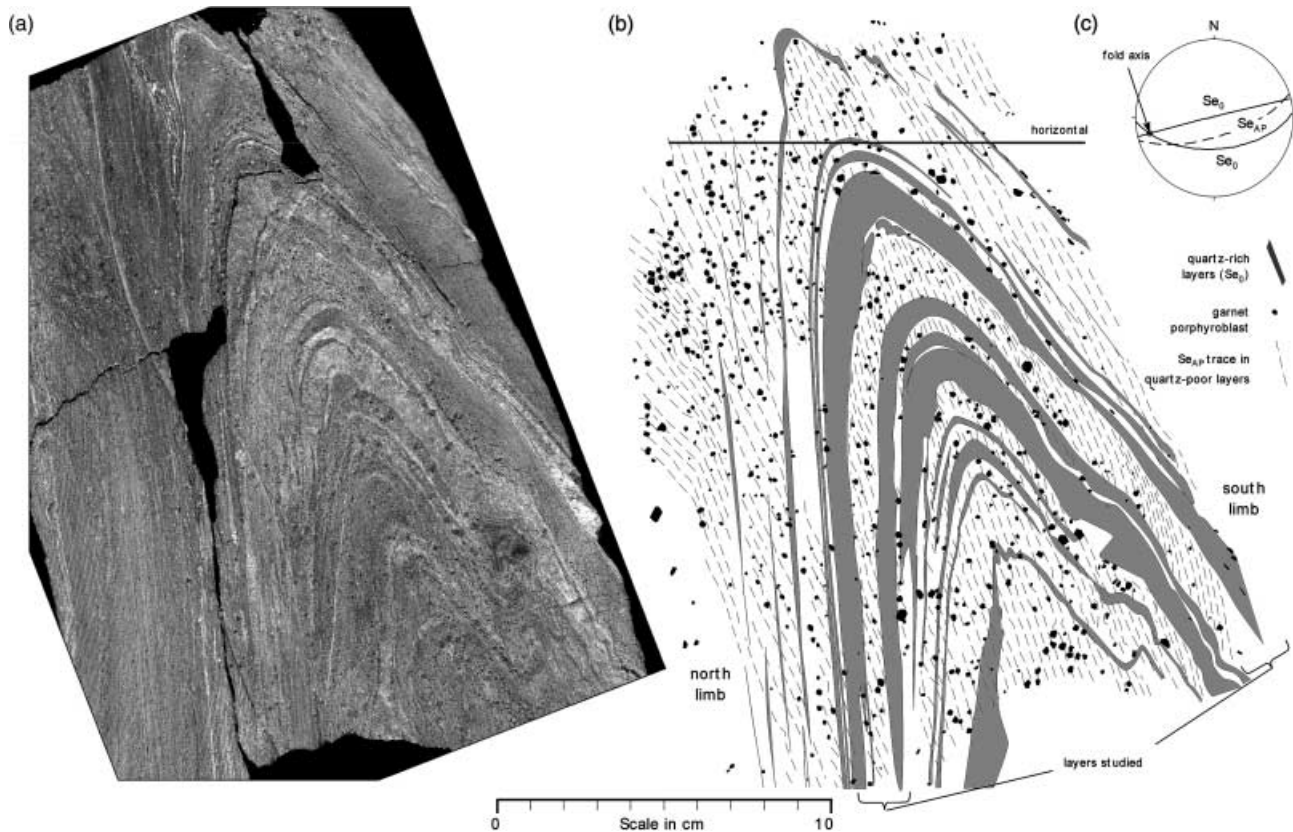


Fig. 4. (a) Photograph and (b) Line diagram of the general geometry of the fold made from a polished slab parallel to the fold profile plane (viewed approximately east). The axial plane strikes ENE–WSW and dips 70° SSE. The axial plunge of the hinge over 50 cm is variable between *c.* 10° to *c.* 30° to WSW. Garnet porphyroblasts occur on both limbs of the fold, and are approximately similar in size and spatial distribution. A clear axial plane (sub) parallel cleavage has developed (Se_{AP}) which crenulates the parallel compositional layering (Se₀) and pervasive schistosity (Se₁). (c) Equal-area stereonet of macroscopic structures of the fold measured in the field. Note how Se_{AP} does not intersect the axis of the fold.

chlorite), and minor late chlorite. All porphyroblasts contain inclusion trails. Biotite porphyroblasts show undulose extinction and abundant asymmetric crystal shapes, suggesting that they have undergone internal deformation probably by slip on the 001 cleavage plane. Therefore, little importance has been placed on the significance of the orientation of these trails because of the potential for re-orientation during internal deformation, and they are not discussed here. Minor chlorite porphyroblasts are inclusion-free and grow across the latest crenulation in mica-rich layers, and are not discussed here.

Description of the garnet porphyroblasts

Garnet porphyroblasts range from *c.* 1–3 mm in diameter (typically *c.* 2 mm) and contain inclusions of ilmenite and fine opaques (graphite?), and less commonly, quartz, which define trails. Garnet forms porphyroblasts with three distinctive habits, which are directly related to their position relative to microstructures. Where garnet lies completely in mica-rich layers (Gr_{t_p}) it forms idioblastic porphyroblasts with

low aspect ratios, typically with sub-rounded crystal faces (Fig. 6). Garnet porphyroblasts that lie adjacent to quartz-rich layers are ‘truncated’ against the quartz-rich layer, and have higher aspect ratios (Gr_{t_{aq}}; Figs 7 & 8). These porphyroblasts locally preserve coarse quartz inclusion trails that form bands that are parallel to truncational margins of the quartz-rich layer. Garnet forms thin tabular porphyroblasts where it occurs in thin pelitic zones between quartz-rich layers (Gr_{t_{qs}}; Fig. 7). A common feature of all except very small garnet porphyroblasts is that they preserve microstructurally distinct core and rims defined by a sharp inflection and change in density of inclusion trails. Idioblastic cores are readily observed, defined by a fine dusting of opaques (graphite?) and ilmenite parallel to crystal faces. Inclusion trails in the core (Si_{1_{core}}) are dominantly straight with increased asymmetric curvature towards the core–rim boundary. Inflection of core trails is partially continuous into a zone of inclusion intensification that defines a crenulation (Si₂), and is preserved only in parts of porphyroblast rims (Fig. 6). In other parts of the rims the equivalent of Si_{1_{core}} (Si_{1_{rim}}) is inflected slightly (Fig. 6). Inclusion

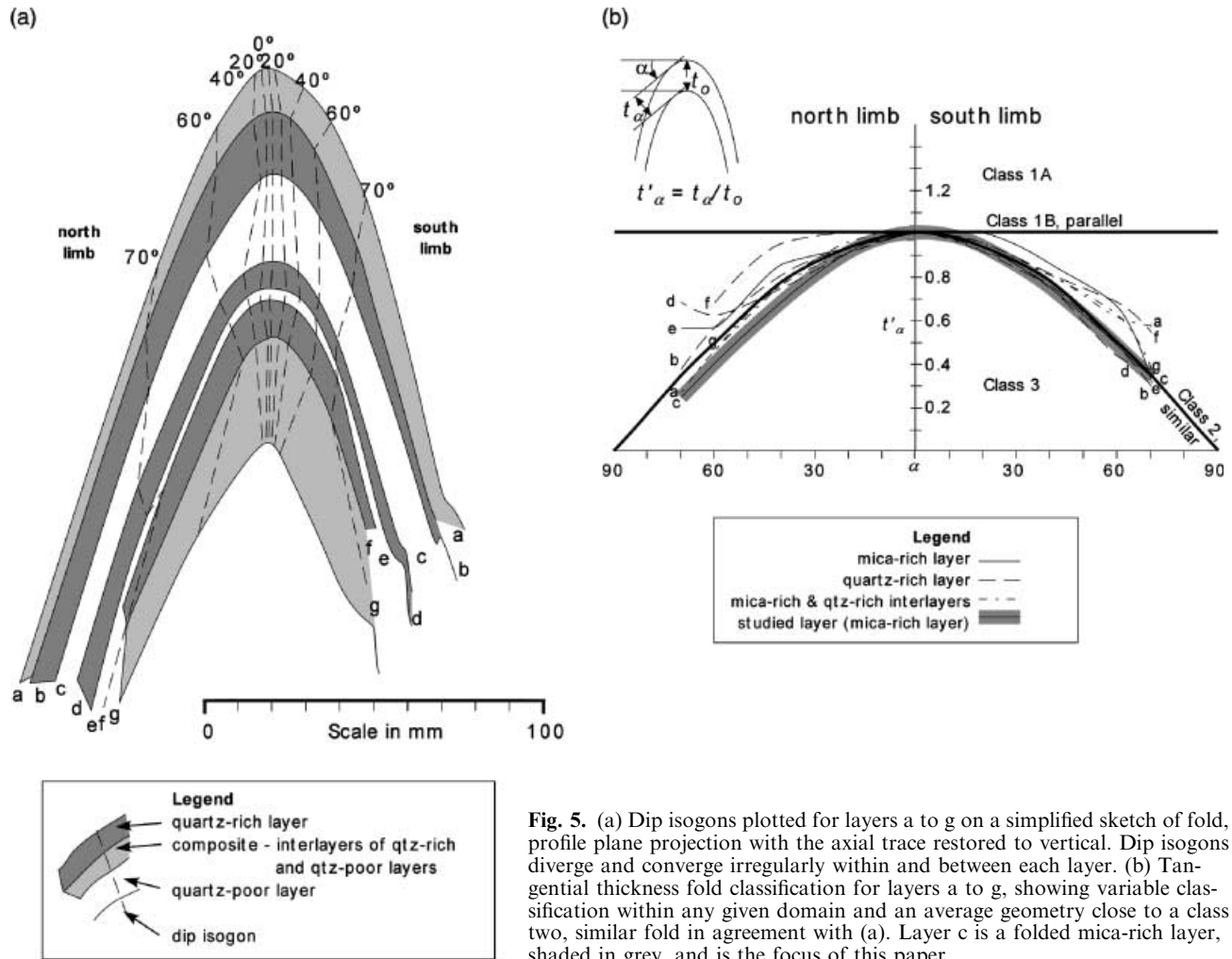


Fig. 5. (a) Dip isogons plotted for layers a to g on a simplified sketch of fold, profile plane projection with the axial trace restored to vertical. Dip isogons diverge and converge irregularly within and between each layer. (b) Tangential thickness fold classification for layers a to g, showing variable classification within any given domain and an average geometry close to a class two, similar fold in agreement with (a). Layer c is a folded mica-rich layer, shaded in grey, and is the focus of this paper.

trails in garnet rims are generally continuous but sharply inflected into matrix microstructures.

Geometric analysis of microstructures in the matrix

Widths of Se_{AP} are variable, but are narrower on the north limb of the fold and mixed layers on both fold limbs, and usually less than the garnet porphyroblasts (Fig. 9). Older crenulations (Se_2) are truncated by Se_{AP} , and are only preserved locally in the strain shadows of porphyroblasts (Fig. 6). These are more apparent on the north limb where the asymmetry differs to Se_{AP} , and can be correlated with Si_2 (see below). The absence of these crenulations and the presence of the well developed, overprinting Se_{AP} outside the strain shadows of the porphyroblasts indicates that these crenulations were probably modified or destroyed outside porphyroblast strain shadows by the development of Se_{AP} . Commonly, Se_{AP} is refracted into parallelism with relatively thick quartz-rich layers where Se_1 has been reactivated and intensified in narrow zones directly adjacent thick quartz-rich layers (Fig. 9). Deformation

microstructures within the quartz-rich layers are texturally less obvious than in mica-rich layers (Figs 7 & 9). In some areas, Se_{AP} continues through thinner quartz-rich layers with minimal diffraction. However, crenulations developed in quartz-rich layers are sparse and heterogeneous (especially in thick quartz-rich layers), and are not well preserved due to the lack of platy minerals in these zones. In thick quartz-rich layers Se_{AP} development has resulted in localised grain-size reduction of quartz. Other zones in quartz-rich layers show evidence of heterogeneous reactivation of Se_1 with a shear-sense antithetic to the bulk fold (Fig. 9).

The standard deviations for Se_{AP} pitch data from the best-fit pole are low, between 5 and 10°, typical of naturally anastomosing foliation surfaces (Timms, 2002). Pitch data for Se_0 has standard deviations of 11.9 and 11.3° for the north and south limbs, respectively (Table 1). These are values typical for 'moderately disturbed planes' (Timms, 2002), which is expected for the limbs of a folded surface. However, the standard deviations for Se_0 pitches directly adjacent garnet porphyroblasts are higher (12.8 &

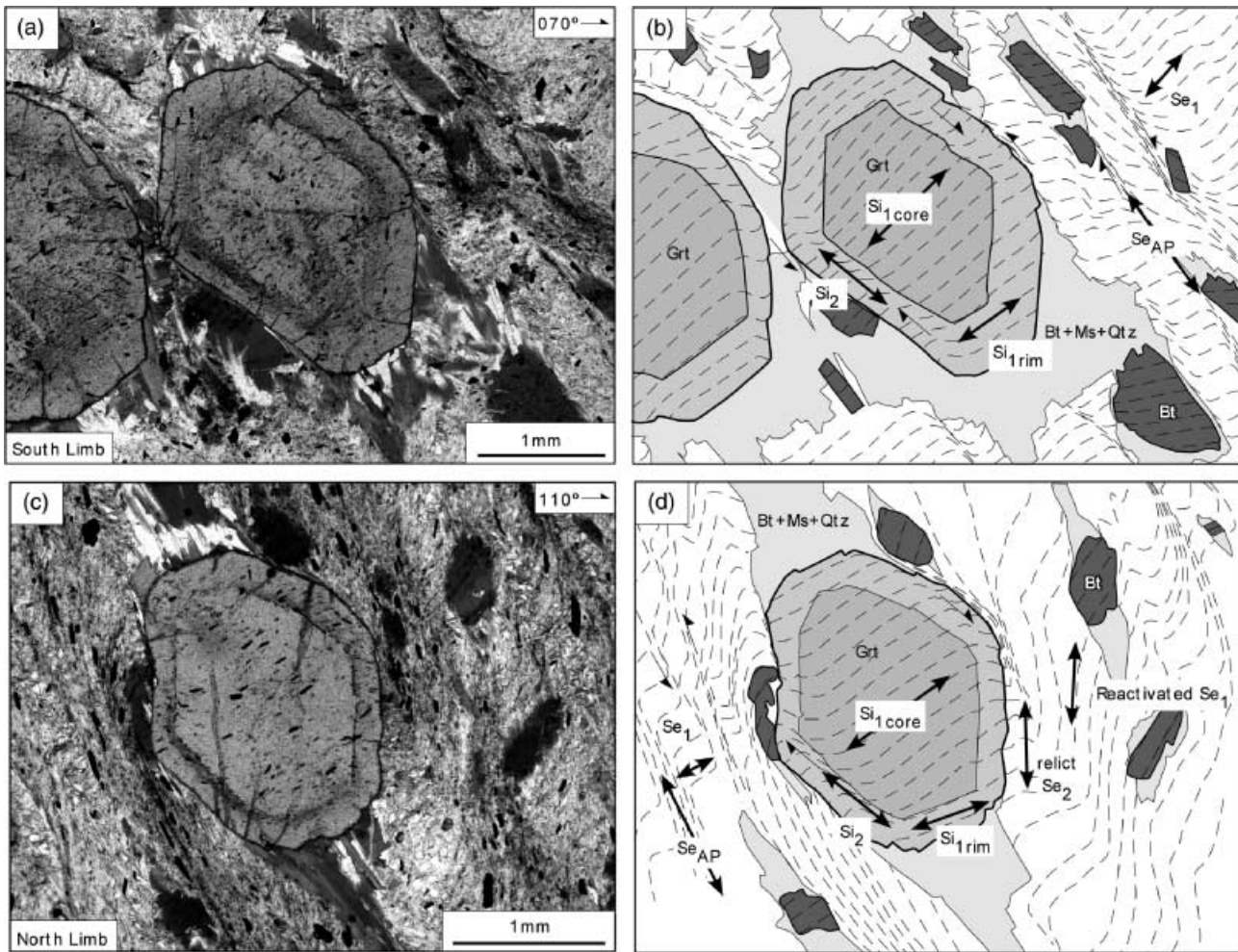


Fig. 6. (a) Photomicrograph and (b) line diagram illustrating garnet (Grt) and the biotite (Bt) porphyroblasts and matrix microstructures on the south limb of the fold. Dominantly straight $Si_{1\text{core}}$ inclusion trails in garnet are inflected clockwise due to core growth (and biotite growth?) during the crenulation event that formed Si_2 . As these crenulations developed they impinged on the porphyroblasts and caused increased inflection of S_1 in the matrix (later to be preserved during rim growth). Garnet rims grew early during an anticlockwise crenulation event, and preserve the slightly re-oriented S_1 and previous crenulations as $Si_{1\text{rim}}$ and Si_2 , respectively. In the matrix, Se_1 has been crenulated clockwise by Se_{AP} , which pitches steeply. Tails of intergrown coarse recrystallized biotite, quartz and muscovite have developed in strain shadows around porphyroblasts, and are elongated parallel with Se_{AP} . 070° striking vertical thin section, south limb, plane polarised light. (c) Photomicrograph and (d) sketch of porphyroblasts and matrix microstructures on the north limb of the fold. Size of porphyroblasts, inclusion trail and matrix textures are very similar to these in (a) and (b). Importantly, the clockwise asymmetry of $Si_{1\text{core}}$ inclusion trails and the anticlockwise asymmetry of inclusion trails at the edge of the rim are the same as the south limb. The main difference is that garnet rim inclusion trails curve continuously into Se_{AP} crenulations in the matrix, which are anticlockwise. Reactivation in the matrix has rotated Se_1 into steeper orientations. 110° striking vertical thin section, north limb, plane polarised light.

15.5°), indicating that they define a surface with increased disturbance (which anastomose more).

Se_0 defines the macroscopic fold, which has a mean interlimb angle of 42° and an axial plunge of $22\text{--}247^\circ$. The local orientation of Se_0 adjacent to garnet porphyroblasts defines an open apparent fold with an interlimb angle of 114° , and an axis oriented at $28\text{--}258^\circ$, slightly oblique to the main Se_0 fold. Se_{AP} developed in mixed layers dips steeply to the SSW, intersects the fold hinge within error, and is within 5° of parallelism on both limbs of the fold (Figs 10 & 11). Interestingly, Se_{AP} developed in mica-rich layers is oblique to Se_{AP} in

mixed layers by approximately 15° in strike, and does not contain the main fold axis (Figs 9, 10 & 11). The attitude of Se_{AP} changes smoothly in the transition zone between mica-rich layers and quartz-dominated layers, and is nearly always of shallower pitch in mica-rich zones in thin section (e.g. Fig. 9). Crenulated Se_1 in the hinges of Se_{AP} are highly variable from crenulation hinge to crenulation hinge and have not been quantified, but locally preserve similar orientations to that of $Si_{1\text{core}}$ (see below; Figs 6 & 7).

The intersection lineation trend for Se_1 and Se_{AP} has been determined using the asymmetry switch method

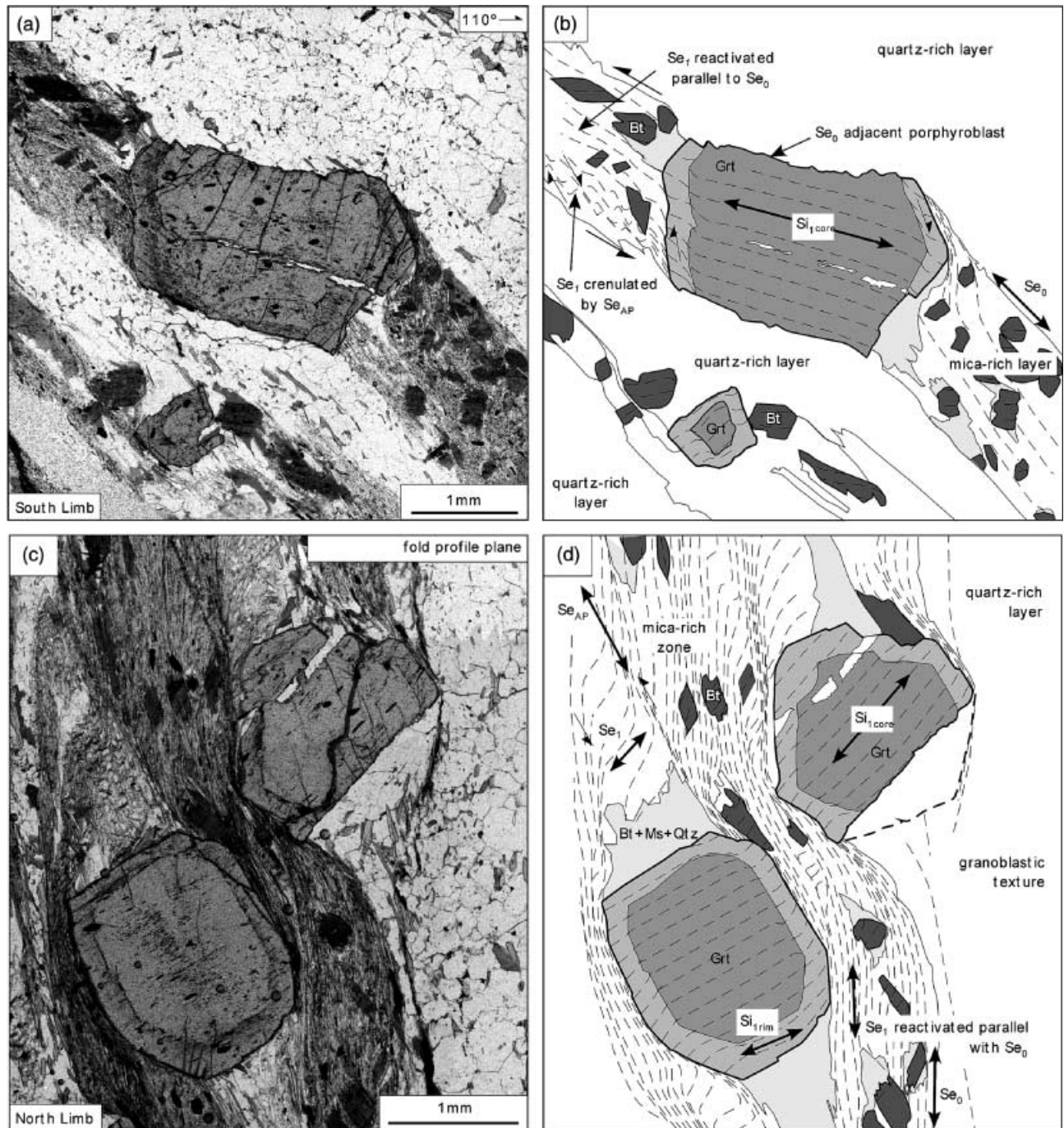


Fig. 7. (a) Photomicrograph and (b) line diagram of a tabular garnet porphyroblast between two quartz-rich layers (Grt_{qs}). Si₁core inclusion trails are inflected clockwise into the rim, and then clockwise into the matrix. Narrow Se_{AP} crenulations are preserved in the matrix only on the left side of image. Elsewhere, the matrix in mica-rich zones has deformed by reactivation of Se₁. Note the angular difference between Se₀ of the quartz-rich layers and Se₀ adjacent to garnet porphyroblast. 110° striking vertical thin section, south limb, plane polarised light. (c) Photomicrograph and (d) interpretative line diagram primarily illustrating garnet porphyroblasts adjacent to a coarse grained quartz-rich zone (Grt_{aq}) and hosted completely within a mica-rich zone (Grt_m). Both garnet porphyroblasts preserve distinctive core and rim zones, with dominantly straight inclusion trails with asymmetric curvature at the edge of each zone. Locally, Se_{AP} crenulations are preserved in the matrix of mica-rich layers, but evidence for reactivation of Se₁ dominates, which has rotated Se₁ into parallelism with Se₀. Fold profile plane thin section, north limb, plane polarised light.

for different composition layers on each limb of the fold (Fig. 12). The intersection lineation trends and angular ranges are different for mica-rich layers vs.

mixed layers, yet very similar in trend in the equivalent layers across the fold. This obliquity between different types of layer broadly coincides with the obliquity of

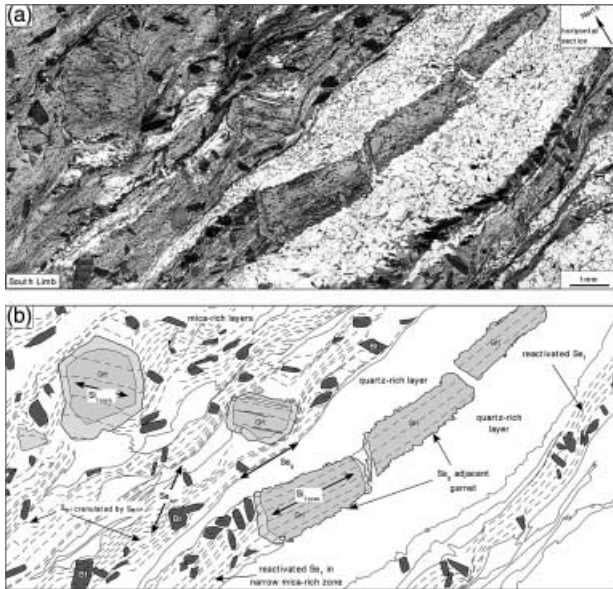


Fig. 8. (a) Photomicrograph and (b) line diagram illustrating garnet porphyroblasts of different morphologies and inclusion trail orientations in spatially different domains. The cores and rims of the porphyroblasts hosted in mica-rich layers are idio-blastic with subrounded crystal faces. Si_{1core} inclusion trails strike NW. The core and rim of the porphyroblast in the centre is truncated on one side adjacent to a thin quartz-rich layer, parallel to Si_{1core} inclusion trails which strike NW. Outside the porphyroblast, the quartz layer is inflected anticlockwise by Se_{AP} crenulation. The three garnet porphyroblasts on the right have grown in a narrow mica-rich layer sandwiched between two quartz-rich layers. The cores and rims of these porphyroblasts are truncated where they have grown against the quartz-rich layers giving them a tabular form. Si_{1core} , Se_1 and Se_0 are locally subparallel here, and all strike WSW. Se_1 in the matrix in these zones has undergone reactivation, which rotated them into parallelism with Se_0 , whereas 'primitive' orientations of Se_1 have been preserved in Se_{AP} crenulation hinges in the mica-rich zones. Horizontal thin section, north limb, plane polarised light.

the strike of Se_{AP} in each type of layer (Fig. 12), and this suggests that the orientation of Se_{AP} controls the orientation of the intersection lineation. This is consistent with Se_{AP} intersecting a gently dipping Se_1 , which, if true, would also indicate that the intersection lineations have shallow plunges. The opposing asymmetries associated with the inflection of the intersections on each limb indicate synthetic bulk shear-sense to the main fold (Fig. 12).

Geometric analysis of microstructures in porphyroblasts

All types of inclusion trails in garnet porphyroblasts preserve surfaces with a lesser degree of planarity than Se_0 and Se_{AP} (Table 1, Figs 10 & 13). Standard deviations range from 11.8 to 18.0°, which are typical values for inclusion trails and are categorised as 'disturbed planes' (Timms, 2002).

Where garnet has grown adjacent to quartz-rich layers Si_{1core} is locally parallel/subparallel to the adjacent quartz-rich layers in all orientations. The

orientation of best-fit great circles for both Si_{1core} and Si_{1rim} of garnet porphyroblasts hosted in mica-rich layers are different on either limb of the fold (Fig. 13). Si_{1core} define an 'apparent' open antiform with a mean interlimb angle of 134° and an axis orientation of 41–279°, which is 32° away from the main fold axis (Fig. 11). Si_{1rim} define an apparent structure that is 5° shallower than this. Planes of best fit from Si_{1core} in garnet porphyroblasts adjacent to quartz-rich layers are oblique to those within mica-rich layers. Si_{1core} in porphyroblasts adjacent to quartz-rich layers define a tighter 'apparent' fold with a mean interlimb angle of 110° and an axis orientation of 34–261°, intermediate between Si_{1core} in the mica-rich layer hosted porphyroblasts and that of the main fold (Fig. 11). Although the planes of best-fit are statistically less constrained for these porphyroblasts, the data are significantly different not to be simply a subset of the dataset for garnet hosted in mica-rich layers. The distribution of Si_2 data is comparable, with near identical best-fit planes that dip moderately to the east on each limb of the fold (Fig. 11).

The distribution of the pitch data and the best-fit great circles of Si_{1core} and Si_{1rim} indicate an approximate 5° shallowing of Si_{1core} to Si_{1rim} on each limb of the fold (Fig. 11). The difference in pitch between Si_{1core} and Si_{1rim} for individual porphyroblasts is heterogeneous on a thin section scale (Fig. 14). For example, in the 140° vertical thin section from the south limb, Si_{1core} pitches are very consistent, whereas Si_{1rim} pitches are variable and steeper (Fig. 14). However, in the spatially adjacent 150° vertical thin section Si_{1core} pitches vary considerably (up to 40°) with < 5° change in the pitch to Si_{1rim} in individual porphyroblasts (Fig. 14). Possible reasons for this are discussed below. Curiously, Si_{1core} and Si_{1rim} of porphyroblasts adjacent to quartz-rich layers in the 140° vertical thin section are highly oblique to those of porphyroblasts hosted in mica-rich layers, and are closer to the mean pitch of Se_0 (Fig. 14).

The FIA for the garnet core is defined by the inflection of Si_{1core} towards Si_2 , and has been constrained by the asymmetry switch and the plane intersection methods for both limbs of the fold. The asymmetry switch method yielded similar trends for the north and south limbs of between 035° + 5°/–35°, and 025° + 55°/–35°, respectively (Fig. 15). The asymmetry switch is coincidental with high frequencies of straight inclusion trails on both limbs. Significantly, the curved foliation defining the garnet core FIA maintains the same asymmetry across the fold, giving a top to the SE shear-sense if the 'non-rotation' model is invoked, or a top to the NW shear-sense using the 'rotation' model. Different FIA plunges have been determined for each limb of the fold. On the south limb the asymmetry switch occurs between 20 and 30° dip to the SSW (Fig. 15). The asymmetry switch on the north limb is more complex, but generally around the horizontal (Fig. 15). However, clockwise, anticlockwise

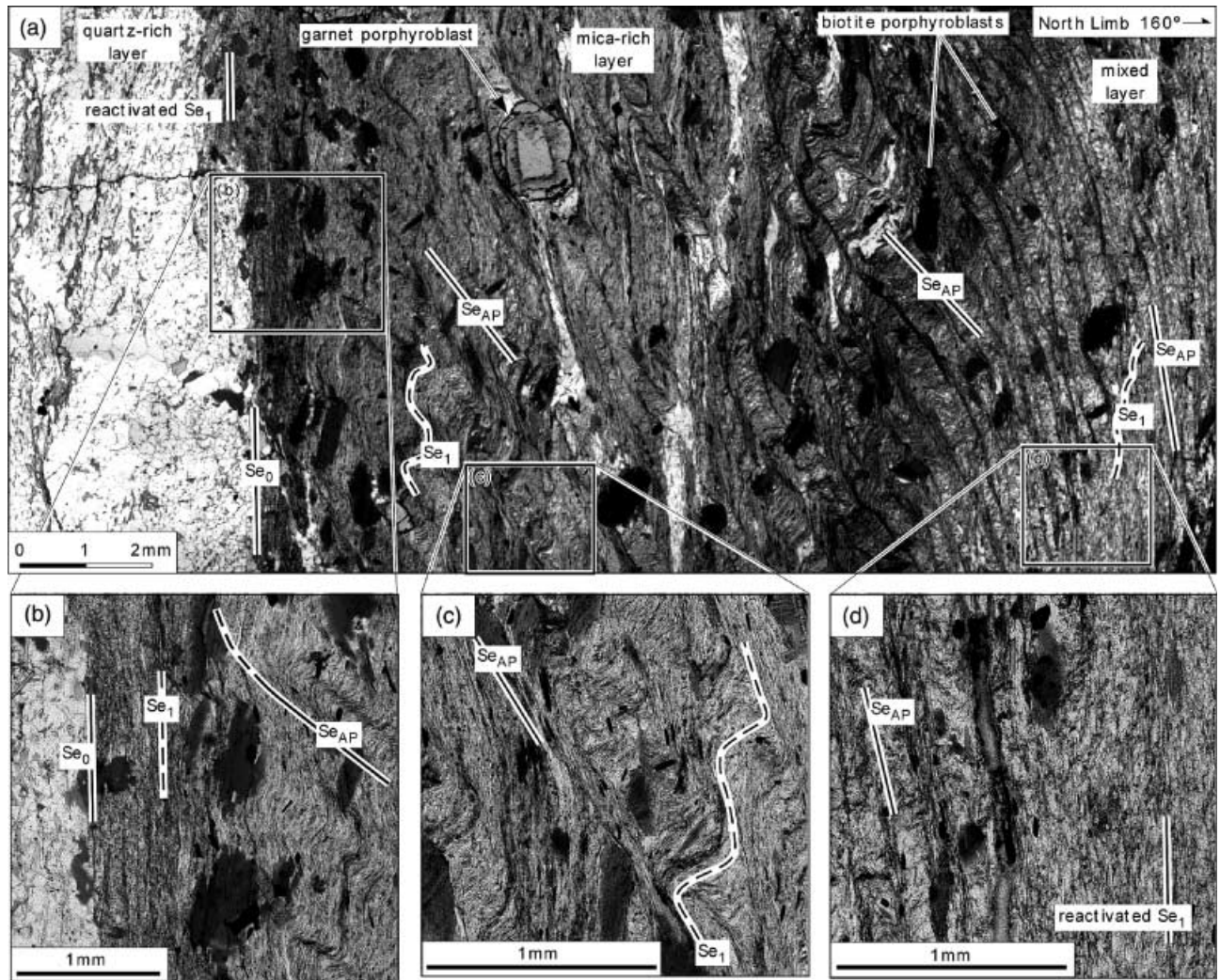


Fig. 9. Photomicrographs illustrating the change in orientation of matrix crenulations in different compositional layers on the north limb of the fold. (a) The field of view spans several layers of different composition. These are, from left to right, a quartz-rich layer with a sharp boundary with a mica-rich layer; gradation into mixed layer, a thin discontinuous quartz-rich layer, then a dark mica-rich layer which is gradational into a mixed layer on the right. Crenulations (Se_{AP}) are clear in mica-rich and mixed layers, but are poorly developed in the quartz-rich layer. Se_{AP} curves smoothly from shallow pitches in mica-rich layers to steeper pitches in quartz-rich layers. (b) A 1-mm wide zone of layer-parallel foliation is observed adjacent the quartz-rich layer. Se_{AP} curve sharply and become less intense into this zone. (c) Se_{AP} crenulations have an anticlockwise asymmetry in the mica-rich layers, which indicates a synthetic shear-sense to the main fold. Generally, Se_{AP} crenulations are widely spaced and have a moderately steep pitch. (d) In the mixed layers, Se_{AP} crenulations also have an anticlockwise asymmetry but have a much steeper pitch and are narrower than in the mica-rich layers. Se_{AP} crenulations become narrower and are near parallel with Se_1 towards the right of the photomicrograph before they disappear. This area, along with the narrow zone in (b), is interpreted to have been dominated by reactivation parallel to Se_1 . The antithetic shear relative to the fold (CW) on the fold limb has rotated them towards Se_1 before they decrenulate as can be readily seen in (b).

and 'millipede' inclusion trails coexist in the same thin sections over a large range of dips on each limb, and the FIA plunge ranges overlap (Fig. 15). The plane intersection method yields slightly different garnet core FIAs for each limb of 19–025° for the north limb and 21–181° for the south limb, which are within the trend and plunge 'range' determined by the asymmetry switch method (Fig. 15). This indicates that each limb has significantly opposing FIA plunges—to the south for the south limb, and to the north on the north limb.

The orientations of inclusion trails in the rims of garnet porphyroblasts are a composite of re-oriented Si_1 , and intensified Si_2 inclusion trails. Commonly, inclusion trails have slight asymmetric inflections into steeper orientations at the very edge of the porphyroblasts (Fig. 6). However, the inclusion trails are commonly truncated by matrix foliations. Therefore, the garnet rim FIA (i.e. the curvature of Si_{1rim} towards the edge of the porphyroblast rims) was determined by the asymmetry switch method, and could not be determined using the plane intersection method

Table 1. Orientation and constraint statistics for matrix foliations (Se) and foliations preserved in porphyroblasts (Si) calculated using pitches from differently oriented thin sections (see text for methods and foliation nomenclature). Statistics calculated using the software Stereoplot (Mancktelow, 1992).

Figure	Microstructure	Fold Limb	Data	Best Pole	Standard Deviation	Data within		Contoured at
						20° of best great circle	10° of best great circle	
Matrix foliations								
6a	Se_0	N	130	04–157	11.9°	88.5%	73.8%	12.5, 17.5, 27.5°
6b	Se_0 (AG)	N	53	46–136	12.8°	90.6%	58.5%	13.6, 19.6, 31.6°
6c	Se_{AP} (M)	N	282	27–336	9.7°	95.7%	78.7%	10.3, 14.3, 22.3°
6d	Se_{AP} (M-Q)	N	149	11–338	5.4°	100.0%	91.9%	5.8, 7.8, 11.8°
6e	Se_0	S	165	34–354	11.3°	93.9%	67.9%	11.9, 16.9, 26.9°
6f	Se_0 (AG)	S	50	55–037	15.5°	70.0%	40.0%	16.3, 23.3, 37.3°
6g	Se_{AP} (M)	S	259	22–331	6.8°	98.8%	87.3%	7.3, 10.3, 16.3°
6h	Se_{AP} (M-Q)	S	128	20–350	7.2°	100.0%	78.9%	7.6, 10.6, 16.6°
Inclusion trails								
7a	Grt Si_{Icore} (M)	N	178	44–134	14.6°	87.1%	51.7%	15.3, 22.3, 36.3°
7b	Grt Si_{Irim} (M)	N	201	51–138	15.4°	81.6%	51.2%	16.2, 23.2, 37.2°
7c	Grt Si_{Icore} (AQ)	N	58	34–144	16.5°	72.4%	39.7%	17.4, 25.4, 41.4°
7d	Grt Si_{Icore} (AQ)	N	47	33–145	18.0°	70.2%	29.8%	18.9, 27.9, 45.9°
7e	Si_2 , all Grt	N	120	40–278	16.2°	80.8%	42.5%	17.0, 25.0, 41.0°
7f	Grt Si_{Icore} (M)	S	234	45–068	12.1°	90.6%	64.5%	12.8, 18.8, 30.8°
7g	Grt Si_{Irim} (M)	S	268	50–068	11.8°	91.0%	62.3%	12.5, 17.5, 27.5°
7h	Grt Si_{Icore} (AQ)	S	93	50–045	18.0°	71.0%	45.2%	18.9, 27.9, 45.9°
7i	Grt Si_{Icore} (AQ)	S	78	54–038	17.4°	69.2%	48.7%	18.2, 26.2, 42.2°
7j	Si_2 , all Grt	S	102	38–288	16.6°	81.4%	54.9%	17.4, 25.4, 41.4°

AG = adjacent garnet porphyroblasts.
M = within mica-rich layers.
M-Q = within mixed quartz-mica layers.
AQ = adjacent quartz-rich layers.

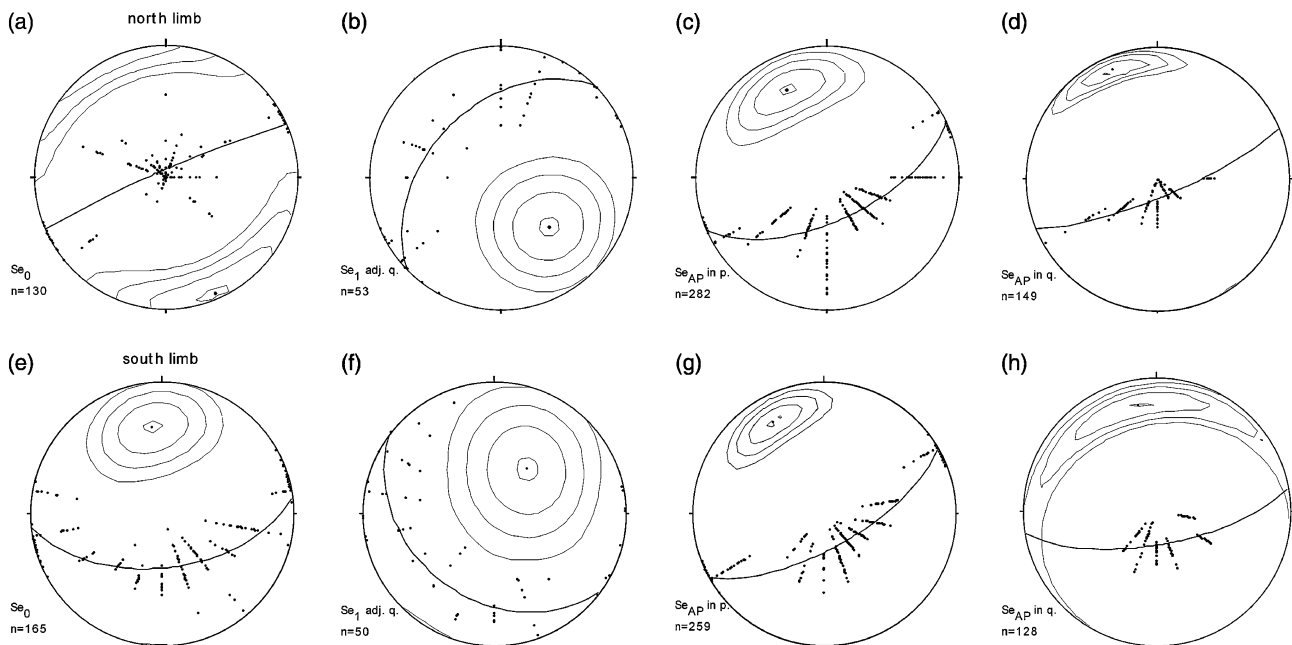


Fig. 10. Equal-area stereonet of matrix foliation surfaces characterised using pitch measurements in differently oriented thin sections. Best-fit great circles, constraint and deviation statistics generated by Stereoplot (Mancktelow, 1992), and are shown in full in Table 1. (a) Macro-scale Se_0 , northern limb. (b) Local Se_0 adjacent to garnet, northern limb. (c) Se_{AP} in mica-rich layers, northern limb. (d) Se_{AP} in mixed layers, northern limb. (e) Macro-scale Se_0 , southern limb. (f) Local Se_0 adjacent to garnet porphyroblasts, southern limb. (g) Se_{AP} in mica-rich layers, southern limb. (h) Se_{AP} in mixed layers, southern limb.

(Fig. 16). Garnet rim FIA trends are very similar with relatively narrow ranges on either side of the fold, and are between 060 and 070° for the north limb, and between 050 and 060° for the south limb (Fig. 16). The asymmetry of the curved inclusion trail surfaces that

define the FIAs remain the same across the fold hinge and hence only match the asymmetry of Se_{AP} on the north limb of the fold. Therefore, the garnet rim FIA is not a result of the inflection of Se_{Irim} by Se_{AP} . The plunge of these FIAs was not measured by the

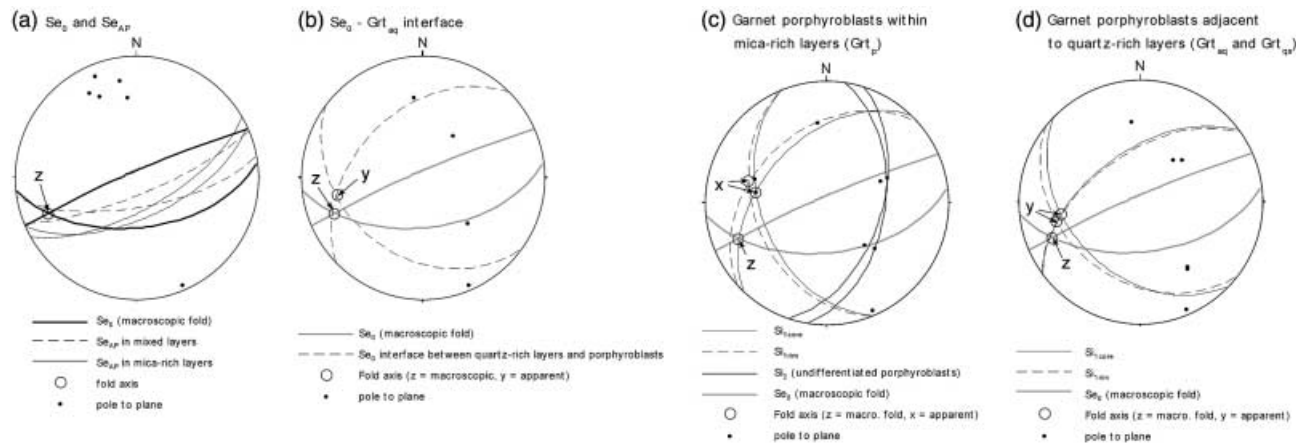


Fig. 11. Equal-area stereonet summarising the surfaces of microstructures shown in Figs 10 and 13. (a) Best-fit planes for matrix foliations of both limbs of the fold. 'z' = fold axis of Se_0 . Notice how Se_{AP} in mica-rich layers transects the fold axial plane in a consistent way, and does not parallel the fold axis 'z', whereas Se_{AP} in mixed layers are closer to the axial plane of the fold. (b) Best-fit planes for interface between garnet porphyroblast and truncational quartz-rich layers, both limbs. This forms an open fold with an apparent fold axis 'y'. (c) Best-fit planes for inclusion trail features of garnet hosted in mica-rich layers, both limbs. Si_{core} and Si_{rim} best-fit planes are very similar on each fold limb. They both define open folds with axes labelled 'x'. Note that the fold axis for Si_{rim} is shallower than that of Si_{core} . 'z' = fold axis of macroscopic fold. (d) Best-fit planes for both Si_{core} and Si_{rim} in garnet porphyroblasts adjacent to quartz-rich layers, both limbs. These inclusion trails define an open fold, both have apparent fold axes labelled 'y', of which Si_{rim} is shallower. 'z' = fold axis of macroscopic fold. See text for further discussion.

asymmetry method, but would have been relatively shallow, representing the intersection of Si_{rim} inclusion trails with a steeply formed crenulation in the matrix (Se_3 ?), which could have been re-orientated or destroyed by subsequent reactivation, possibly during the formation of Se_{AP} .

INTERPRETATION

Deformation history of the matrix

The quartz-rich layers could be relict original compositional layering, or could have been formed tectonically. Understanding their origin and timing relative to other structures is important for determining the complete deformation history of the sample. The coarse grain size and granoblastic textures in the quartz-rich layers suggest a period of grain growth, which may or may not be related to their genesis. The quartz-rich layers could be the result of recrystallization of laterally discontinuous quartz-rich compositional layering, or the result of extreme deformation partitioning (e.g. stage 5 in crenulation development; Bell *et al.*, 1986). However, the presence of thicker, layer-parallel quartz veins in the vicinity of the fold suggests that the quartz-rich layers were originally veins parallel to compositional layering, and have been folded to their present orientation. Textural evidence suggests that a strong pervasive foliation existed parallel to- and within the veins and layers, the relicts of which now form Se_1 in mica-rich and mixed layers. Therefore, the quartz-rich veins were formed early in the deformation history, and the development of Se_1 is the first foliation preserved in

the matrix. The presence of the quartz-rich layers during folding is very significant for the deformation history of the fold. It could be expected that, with respect to the quartz-poor layers, the quartz-rich layers would have behaved mechanically differently at different times. For example, crenulation development may have been inefficient in these layers, which could have been mechanically stronger than adjacent mica-rich layers. If this were so, folding may have been accommodated by layer-parallel shearing, which would have been more intense in quartz-poor layers. Alternatively, coupled crenulation development in quartz-poor layers and layer-parallel shearing in the quartz-rich layers. The likelihood of these scenarios is discussed below.

From analogue modelling and many natural examples, strain in multilayer folds is expected to be concentrated in the less competent layers which tend to form class 3 folds, whereas competent layers form parallel, class 1b folds (Ramberg, 1964; Ramsay, 1967; De Bremaeker & Brecker, 1978). In this situation, the incompetent layers undergo strong shearing parallel to layering and flattening approximately normal to them. The combined geometry of a competent/incompetent layer pair approximates that of a similar, class 2 fold. However, the individual mica-rich and quartz-rich layers in the fold in this study do not form markedly different geometries, and approximate similar class 2 folds. Therefore, it is difficult to tell whether strain has been concentrated into either the quartz-rich layers or the mica-rich layers (or neither) using the bulk geometry alone. Other microstructures have to be examined to determine how strain was partitioned within the mica-rich or the quartz-rich layers. It is clear from the

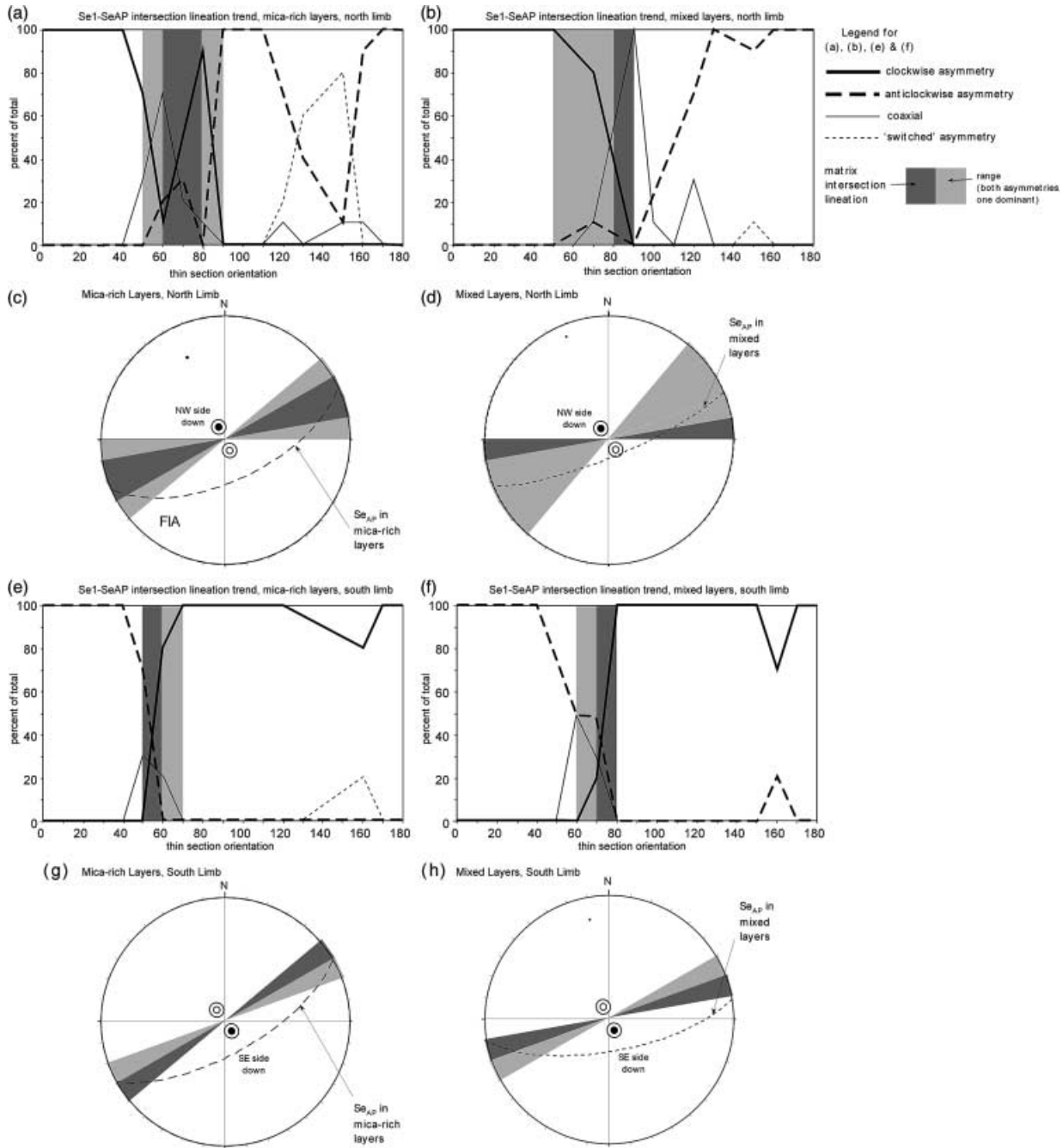


Fig. 12. The matrix intersection lineation for Se_1 and Se_{AP} determined by the asymmetry switch method (see text) for different parts of the fold on both limbs. (a) Intersection lineation trend constraint for Se_1 and Se_{AP} in mica-rich layers on the north limb. (b) Intersection lineation trend constraint for Se_1 and Se_{AP} in the mixed layers on the south limb. (c) and (d) Equal-area stereoplots of intersection lineations determined in (a) and (b). (e) Intersection lineation trend constraint for Se_1 and Se_{AP} in mica-rich layers on the south limb. (f) Intersection lineation trend constraint for Se_1 and Se_{AP} in the mixed layers on the south limb. (g) and (h) Equal-area stereoplots of intersection lineations determined in (e) and (f). Generally, the lineations in equivalent layer types on each limb of the fold are parallel. However, there are subtle differences in the trends between different layer types. Intersection lineations trend around 060° in mica-rich layers, but is offset in the mixed layers to between 070 and 090° . All of the lineations have overlapping angular ranges. Importantly, mixed layers have noticeable one-sided angular range distributions, where both asymmetries persist to more NE–SW trends. The asymmetry of the intersection lineations are opposite on either side of the fold, with a synthetic shear-sense to that of the main fold. The plunges of matrix intersection lineations have not been determined. However, the best-fit planes for the relevant surfaces have been plotted on to the appropriate stereonet for comparison of trends with the lineations. The trends of the best-fit planes are remarkably similar to the intersection lineation trends, which is consistent with a gently dipping foliation overprinted by the steeply dipping Se_{AP} . This indicates that the intersection lineations possibly have relatively shallow plunges. Further discussion pertaining to this figure is contained in the text.

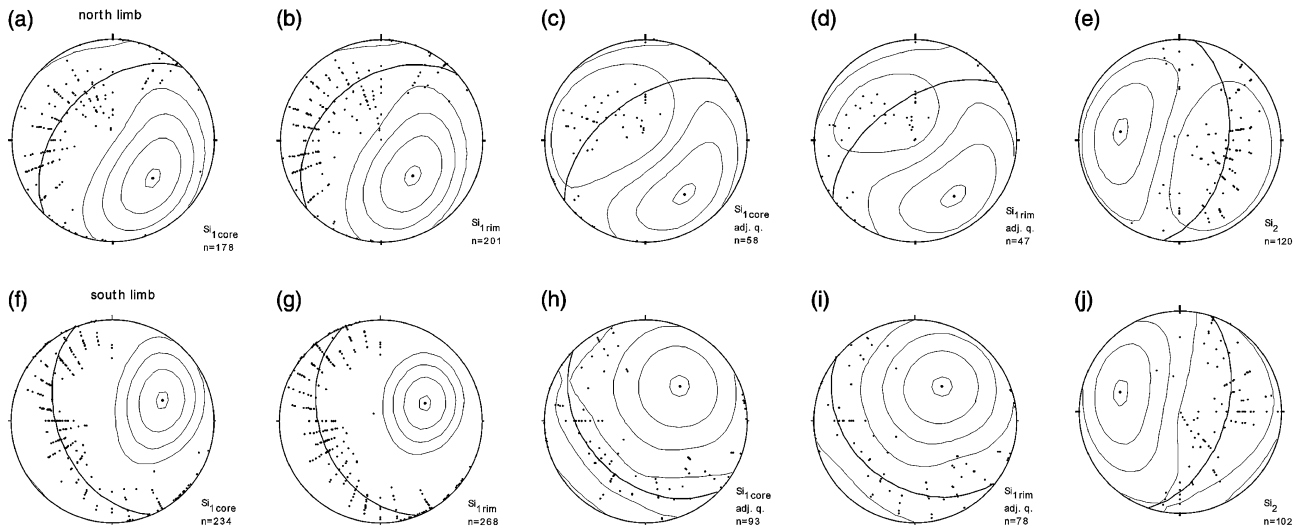


Fig. 13. Equal-area stereonet projections of inclusion trail surfaces estimated from pitch measurements in differently oriented thin sections. Best-fit great circles and angular contours generated by Stereoplot (Mancktelow, 1992). Related orientation and statistical data are shown in Table 1. (a) $Si_{1\text{core}}$ in garnet porphyroblasts hosted in mica-rich layers, north limb. (b) $Si_{1\text{rim}}$ in garnet porphyroblasts hosted in mica-rich layers, north limb. (c) $Si_{1\text{core}}$ in garnet adjacent quartz-rich layers, north limb. (d) $Si_{1\text{rim}}$ in garnet porphyroblasts adjacent quartz-rich layers, north limb. (e) Si_2 in all garnet porphyroblasts, north limb. (f) $Si_{1\text{core}}$ in garnet porphyroblasts hosted in mica-rich layers, south limb. (g) $Si_{1\text{rim}}$ in garnet porphyroblasts hosted in mica-rich layers, south limb. (h) $Si_{1\text{core}}$ in garnet porphyroblasts adjacent quartz-rich layers, south limb. (i) $Si_{1\text{rim}}$ in garnet porphyroblasts quartz-rich layers, southern limb. (j) Si_2 in all garnet porphyroblasts, south limb.

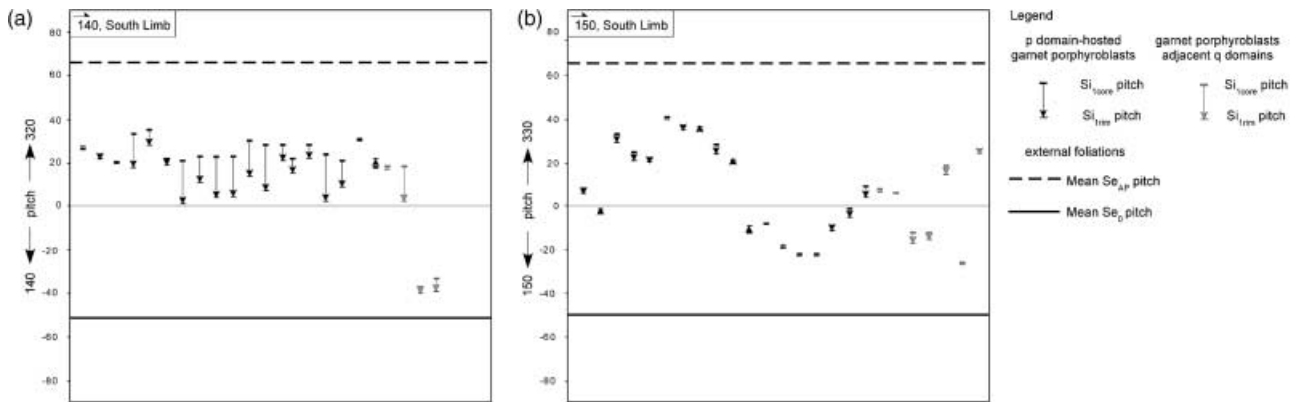


Fig. 14. A comparison of $Si_{1\text{core}}$ and $Si_{1\text{rim}}$ pitches in individual garnet porphyroblasts across two orientated vertical thin sections. Only data where $Si_{1\text{core}}$ and $Si_{1\text{rim}}$ in individual porphyroblasts were measured have been plotted. The x-axis corresponds to left-to-right transect of the thin section. (a) 140° section, southern limb. (b) 150° section, southern limb. The mean pitch of Se_0 has not been plotted, but for (a) is *c.* 52° , and (b) is *c.* 47° to the SE.

preservation of different types of microstructure in different parts of the fold that deformation was partitioned at several scales during folding, quite possibly at different times. The style and location of deformation partitioning is important for the expected porphyroblast behaviour.

Se_{AP} truncates early crenulations preserved only in strain shadows around porphyroblasts, which is evidence of deformation partitioning in the matrix prior to Se_{AP} development. These crenulations do not change asymmetry across the main fold, and in some places are continuous with Si_2 in the rims of garnet

porphyroblasts. Therefore, it is interpreted that these relict crenulations are the same microstructure as Si_2 .

In mica-rich and mixed layers, deformation was partitioned effectively and a steeply dipping crenulation cleavage (Se_{AP}) developed and is well preserved. Se_{AP} in mixed layers is parallel (within error) to the fold axis and has the same bulk asymmetry as the main fold, which is evidence for formation of Se_{AP} during folding. The obliquity of Se_{AP} between the mica-rich layers vs. the mixed layers is not simply 'refraction' of the cleavage through rheologically different layers during fold development. If this was

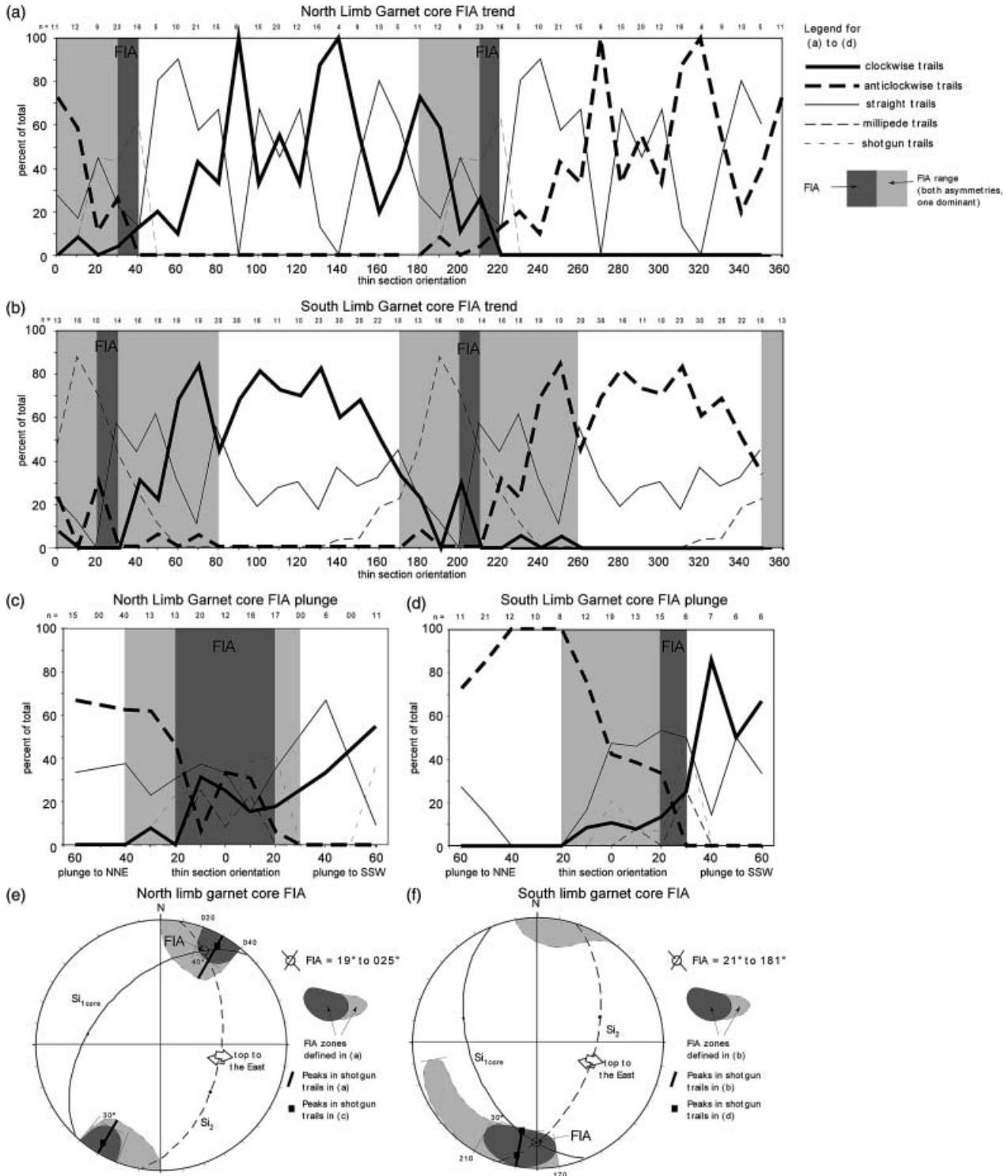


Fig. 15. Orientation of foliation intersection axes (FIA) of Si_{1core} - Si_2 in all garnet porphyroblasts as determined by the asymmetry switch method and the plane intersection method. (a) Si_{1core} - Si_2 FIA trend constraint for the northern limb by the asymmetry method. (b) Si_{1core} - Si_2 FIA trend constraint for the southern limb by the asymmetry method. Asymmetries on vertical thin sections viewed with orientation direction consistently to the right. (c) Si_{1core} - Si_2 FIA plunge constraint for the northern limb by the asymmetry method. Thin section orientations plunge within the 030° plane. (d) Si_{1core} - Si_2 FIA plunge constraint for the southern limb by the asymmetry method. Thin section orientations plunge within 020° plane. Si_{1core} asymmetries measured for plunge determination on thin sections viewed from above. (e) & (f) Equal-area stereonets with best-fit great circles for Si_{1core} and Si_2 on the northern limb and the southern limb, respectively. The FIA calculated from the plane-intersection method is circled. FIA range zones (grey fields) correspond closely to those calculated from the asymmetry method.

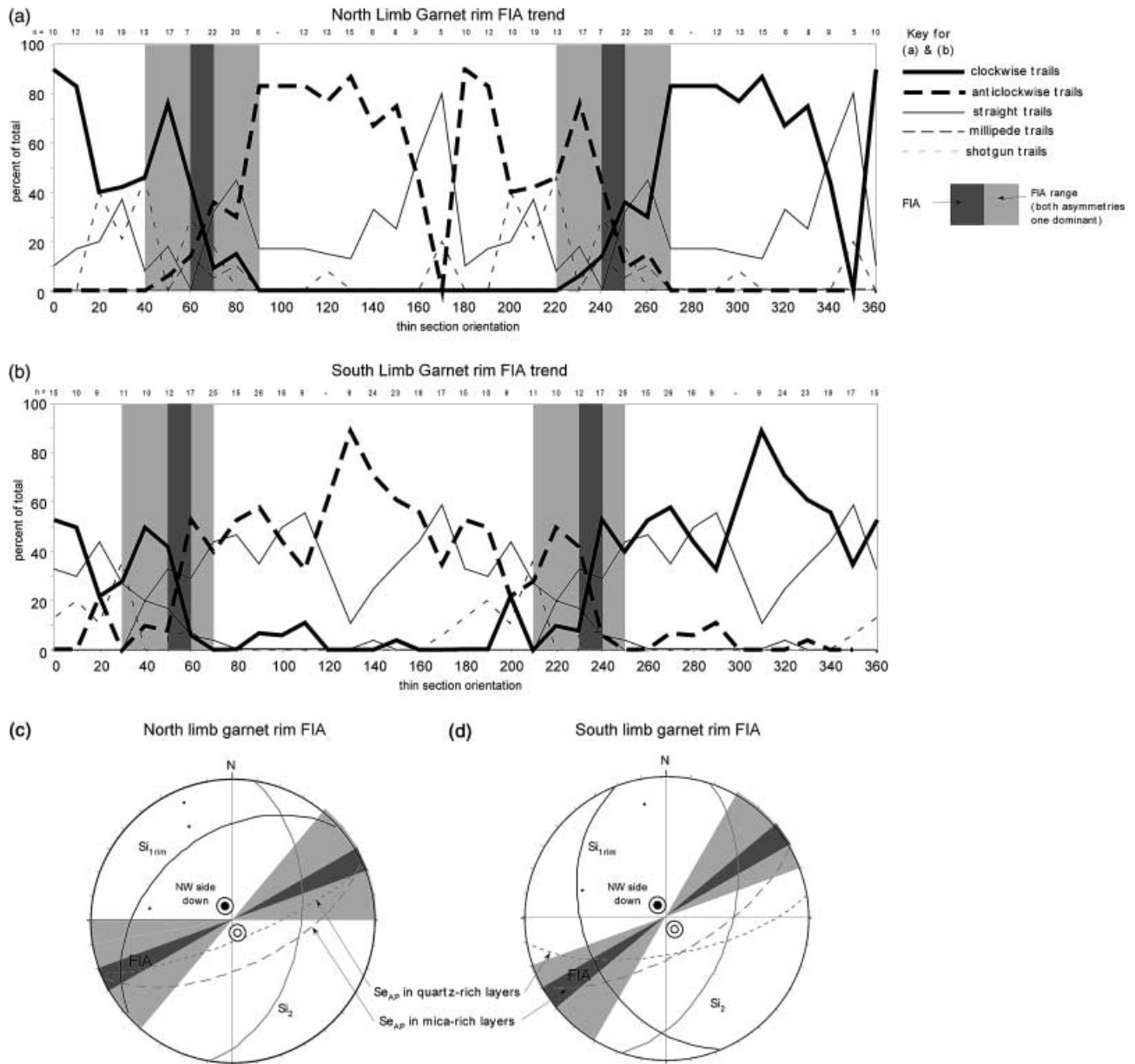


Fig. 16. Si_{1rim} -matrix FIA of all garnet porphyroblasts constrained by the 'asymmetry switch' and the 'plane intersection' methods (see text) for each limb of the fold. (a) Si_{1rim} -matrix FIA trend constraint for the northern limb by the asymmetry method. (b) Si_{1rim} -matrix FIA trend constraint for the southern limb by the asymmetry method. Asymmetries on vertical thin sections viewed with orientation direction consistently to the right. The plunge of the garnet rim FIA was not measured by the asymmetry switch technique. (c) & (d) Si_{1rim} -matrix FIA calculated using the plane intersection method. Equal-area stereonet with best-fit great circles for Si_2 and Se_{AP} on the northern limb and the southern limb, respectively. The rim FIA is the inflection of Si_{1rim} by S_3 (not shown or measured), and has been determined using the intersection of Si_{1rim} and the FIA trend calculated from the asymmetry method (indicated by the grey zones). The trend of the rim FIA is similar in all compositional zones, and on each limb of the fold, and plunges very gently on the north limb, and moderately on the south limb.

correct, in three-dimensions, cleavages formed in similar layers on either limb synchronous with folding should be orientated symmetrical to, and intersect the main fold axial plane when plotted on a stereonet. However, the orientation of Se_{AP} in mica-rich layers transects the fold on each limb in a consistent orientation, which is problematic for a simple 'single stage'

development of Se_{AP} (Fig. 11). A more satisfactory explanation is that Se_{AP} has been modified since its formation in some domains/layers. In detail, Se_{AP} crenulations are most clearly preserved in mica-rich layers, whereas they are narrow in mixed layers and are not crenulated in quartz-rich layers (Fig. 9). This is particularly obvious on the left side of Fig. 9. It is

interpreted that the orientation of Se_{AP} in mixed and quartz-rich layers has been modified by reactivation synchronous to the folding of layering to the present orientation. Reactivation was inefficient in the mica-rich layers due to the presence of significantly more porphyroblasts. Deformation was partitioned around the mica-rich layers, which has preserved the original orientation of an earlier-formed Se_{AP} . Importantly, this suggests additional complexity of matrix development during the development of the fold.

In the narrow zones adjacent to quartz-rich layers, deformation partitioning was less effective on the scale of the porphyroblasts and narrow zones of intensified foliation (reactivated Se_1) developed parallel to layering caused by focused layer parallel shearing (Fig. 9). This is likely due to contrasting rheology between different composition layers. In these zones Se_{AP} crenulations are inflected towards parallelism with reactivated Se_1 . Generally, the coarser grain size of most parts the quartz-rich layers suggest that these were strong zones, and that there was less internal strain in parts of the quartz-rich layers.

Timing of porphyroblast nucleation and growth

The similarity between textures and size of garnet porphyroblasts on either limb of the fold suggests that cores nucleated on both limbs at the same time. Commonly, small garnet porphyroblasts do not show a textural core–rim boundary. This relationship is expected for 2-D sampling of a population of similar-sized porphyroblasts with common, characteristic core–rim textures. This suggests that the differences in grain size in thin section are due to a ‘cut effect’, and is consistent with the assumption that all the garnet porphyroblast cores nucleated at the same time, and that the rims developed synchronously later. Therefore, all of the porphyroblasts from both limbs form two populations, each of which is temporarily equivalent, core-to-core, and rim-to-rim, respectively.

The timing of porphyroblast growth relative to other structures is crucial to the understanding of their behaviour during deformation. Inclusion trail inflections at core–rim boundary and at the very edge of the garnet porphyroblasts suggest that FIAs develop synchronous with porphyroblast growth and therefore the orientations of FIAs and inclusion trails from either limb of the fold can be compared directly. Generally, garnet core and rim FIAs are oblique to the fold axis, pre-date the formation of Se_{AP} , and preserve the same asymmetry across the fold. Initially, this suggests that garnet core growth pre-dates and is unrelated to the main fold. However, subtle differences in the trend, plunge, and ranges of the garnet core FIA from limb to limb appear to be related to the bulk geometry of the fold. This can be explained in different ways, and is discussed below.

Once foliations are trapped within garnet porphyroblasts as inclusion trails they no longer behave as

material lines as they would in the matrix. Instead, their orientation is a culmination of the orientation of the matrix foliation at the time of garnet growth plus the effect of post-growth garnet rotation. Therefore, if initial parallelism of inclusion surfaces in time equivalent porphyroblasts and homogeneity of deformation in the matrix is assumed, differences in inclusion surface orientation can be used to infer rotation relative to each other. Garnet cores and rims have overgrown foliations Si_1 and Si_2 with varying degrees of planarity. The variable distribution of pitch data for all inclusion trails could be explained by models involving rotation, or non-rotation of porphyroblasts, relative to each other, or external reference frames. Although the differences between the models seem quite subtle, each model provides profoundly different interpretations of timing of porphyroblast growth and fold development (Fig. 17). The validity of interpretations from each model is discussed below.

DISCUSSION

Porphyroblast timing and behaviour in the non-rotation model

If porphyroblasts did not rotate, the geometry of inclusion trails would represent the pre-growth foliation geometry, and would provide a very useful record of early foliation orientations. In this model, variations in inclusion trail orientations between adjacent porphyroblasts have important implications for the timing of nucleation with respect to crenulation development, and to the timing of folding (Fig. 17). The FIA orientations indicate that the garnet cores grew synchronously with the development of a NNE–SSW trending foliation event with consistent E-down shear sense (S2), and garnet rims grew synchronously with development of a steeply dipping, NE–SW trending foliation event with consistent NW-down shear sense (S3). The variation in the attitude of Si_{1core} between adjacent porphyroblasts in the same thin section can only be explained by orientation differences before porphyroblast growth. This can be accounted for by either difference in porphyroblast nucleation timing during active crenulation of Si_1 , or synchronous porphyroblast nucleation over Si_1 in crenulation hinges or over limbs that were heterogeneously developed. The data distribution alone is an insufficient criterion for differentiating between the non-rotation and the rotation models. Regardless of nucleation timing, some pitches of Si_{1core} would represent ‘primitive’ orientations of Si_{1core} before crenulation, whereas others would represent pre-porphyroblast foliations variably rotated by Si_2 . In a similar way, orientations of Si_{1rim} would reflect a local composite of the pre- and post-core growth rotational effects due to the Si_2 event, combined with the pre-rim rotational effects of Se_1 due to the steeply dipping crenulation event that formed S3 synchronous to rim

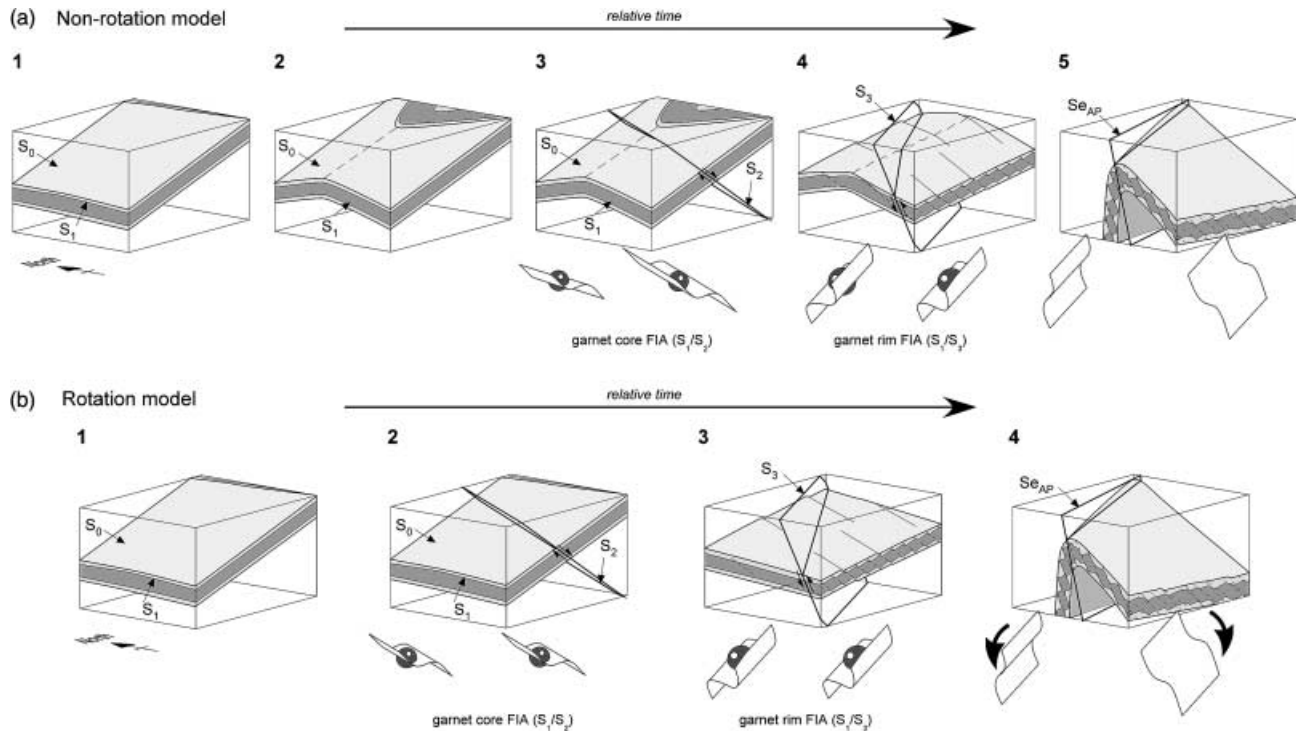


Fig. 17. A series of interpretative block diagrams showing the evolution of the fold, and timing of the development of matrix structures and garnet porphyroblasts for (a) a non-rotation model and (b) a rotation model. The fold has been simplified to a single mica-rich layer, with top and bottom surfaces representing interfaces with quartz-rich layers. Additional annotation diagrams to show asymmetric structures are included where appropriate. Generally, the relative deformation histories are similar for each model, except for the addition of a pre-porphyroblast upright open ENE–WSW trending folding stage to explain the inclusion trail geometry in the non-rotation model. In the non-rotation model, development of Se_{AP} was synthetic to the pre-existing bulk fold, which tightened the limbs and re-orientated the hinge anticlockwise. In the rotation model, some porphyroblasts were rotated during the development of Se_{AP} and the antiform.

growth. The orientation of porphyroblast crystal faces would have locally controlled the pitch of intensified S_2 against the porphyroblast, but is predominantly a product of deformation partitioning. This S_2 is sometimes included in the rim, which grew later during the formation of S_3 (Fig. 17a4). A lack of rotation of porphyroblasts relative to each other, or any other reference frame would suggest that the open fold defined by Si_{1core} inclusion trails was present before porphyroblast growth (Fig. 17a). It would also suggest the presence of the tighter fold defined by Se_0 pitches adjacent to tabular porphyroblasts, prior to garnet core growth. If this is correct, and garnet core growth was relatively synchronous on each limb as the data suggests, then deformation partitioning accompanying folding must have been present in the matrix prior to core growth to explain the difference between Si_{1core} orientation in porphyroblasts adjacent to quartz-rich layers and in mica-rich layers. If porphyroblast nucleation was not initiated until the development of Si_2 , deformation partitioning must have been weak and widely spaced during the early open fold formation, otherwise relict disruption and curvature of foliation surfaces from this event would be preserved in garnet cores, thus increasing the angular range over which

both asymmetries are present, which is not consistent with the observed inclusion trail asymmetry data. Therefore, the difference in the orientation of Si_{1core} on each limb between Gr_{tp} and Gr_{qs} is difficult to explain in the non-rotation model, and a model involving absolutely no rotation is considered unlikely.

Porphyroblast timing and behaviour in the rotation model

In the rotation model, the variable orientations of inclusion trail pitch in a single thin section would indicate heterogeneous rotation of porphyroblasts relative to each other at any time after growth. If rotation occurred before rim growth then variable Si_{1core} pitch, but consistent Si_{1rim} pitch would be expected, and therefore variable angular difference between Si_{1core} and Si_{1rim} . However, Si_{1rim} pitches mimic those of Si_{1core} for individual porphyroblasts within a given thin section orientation, and have a mean angular difference of 5° for all thin section orientations, which is consistent with heterogeneous rotation relative to each other after garnet rim growth.

The difference in Si_{1core} and Si_{1rim} orientation and difference in garnet core FIA orientation from limb to limb could be explained by bulk rotation of porphyro-

blasts (with shallowly dipping inclusion surfaces) in opposite directions on each fold limb about axes at 41–279° for the mica-rich zones, and 34–261° for the quartz-rich zones ('x' and 'y' on Fig. 11). This axis is oblique to north by 32° of the main fold axis for porphyroblasts hosted in mica-rich layers, and 17° north for those adjacent to quartz-rich layers. If rotation of porphyroblasts had occurred about this axis on each limb of the fold, data would be distributed along small circles on a stereonet about axis 'x' and 'y' (Fig. 11). Curiously, the best-fit great circles for Si_2 are almost perpendicular to these axes, and therefore no effective change in Si_2 orientation would be expected if garnet porphyroblasts rotated after the formation and inclusion of S2 into the rims. A change in the plunge of the garnet core FIAs would be expected between limbs, consistent with observations. However, the garnet rim FIAs are much closer to the main fold axis (Figs 11 & 16). Therefore, rotation magnitudes would have been much less than that of the core FIAs if rotation had occurred after porphyroblast growth. This is consistent with observations, in which garnet rim FIAs remain close to parallel across the fold (Fig. 16). The axes of apparent rotation do not lie within the axial plane of the fold (Fig. 11). In three-dimensions, the axis of rotation for the porphyroblasts should lie within a theoretical 'flow plane'. For example, the axis of the fold limbs lie within the axial plane – the flow plane of the fold if it formed by axial slip. All flow planes of the main folding event must contain the fold axis. Therefore, the data are incompatible with rotation of porphyroblasts after growth caused by the development of Se_{AP} during the main folding event. If porphyroblast rotation had occurred during upright folding after porphyroblast core growth, reorientation of the apparent fold limbs defined by Si_{core} would have occurred. This upright folding was about an axis oblique to the apparent Si_{core} fold (as the data suggests), and would have resulted in changes dominantly of the axial plunge of the Si_{core} fold. In this situation, rotation of the axial trend of the apparent fold defined by Si_{core} would have been difficult during deformation subsequent to garnet core growth. In the rotation model, the macroscopic fold geometry has a longer resetting time-scale to that of the inclusion trails in porphyroblasts. The misalignments between the main fold axis and the apparent fold axes defined by inclusion trails in garnet porphyroblasts are 32° for Grt_p and 17° for Grt_{aq} and Grt_{qs} . Therefore, it could be argued that these misalignments are due to the porphyroblasts rotating relative to the axial plane progressively with different velocities during variations in the orientations of the applied stress field over the life of the fold. If there were variations in the applied stress field over the life of the fold causing fold hinge rotation, then the 'flow plane' of the fold should have also varied over time, resulting in the observed misalignment between the macroscopic fold axis and the axes of apparent rotation (z, x and y of Fig. 11). This is in

agreement with the interpretation that Grt_{aq} and Grt_{qs} have rotated during folding more than Grt_p if the degree of rotation was a function of layer composition and hence deformation partitioning. Further, the foliation event in which the garnet rims grew (S3) could have been an early equivalent of Se_{AP} , that formed before the progressive switch of the flow plane towards the actual position, so that the asymmetry of the inclusion trails remained the same across the fold.

The most likely deformation history is as follows: The growth of garnet cores was synchronous with the development of S2 crenulations, which are highly oblique to the present fold orientation and have an E-down shear-sense (Fig. 17b2). NW–SE bulk shortening initiated development of Se_3 crenulations slightly oblique to the pre-existing fold. Se_3 formation was accompanied by garnet rim growth (Fig. 17b3). The N-down shear-sense of Se_3 produced the consistent asymmetry for the garnet rim FIA. As deformation progressed, the shear-sense of Se_3 crenulations locally switched to S-down to produce Se_{AP} and the antiform (Fig. 17b4). Garnet growth had ceased by this stage, and deformation became increasingly noncoaxial as the fold limbs became steeper and some garnet porphyroblasts rotated with them. Reactivation of $Se_{0,1}$ and Se_{AP} dominated over crenulation, and consequently the fold was tightened to its present orientation.

The importance of 3D geometric analysis of inclusion trails and foliations

In many previous studies, the conventional way of fold analysis has been to observe structures on a plane perpendicular to the fold axis, known as the fold profile plane, and assume plane strain. In this study the axis of apparent rotation does not coincide with the macro-fold axis and is misaligned by about 15°. If the microstructures in the porphyroblasts and matrix of this fold were only observed in two dimensions, then the 'apparent' open fold defined by garnet core inclusion trails could lead to erroneous interpretations of porphyroblast rotation relative to the fold axial plane.

SUMMARY AND CONCLUSIONS

- (1) Microstructures preserved in the porphyroblasts and in the matrix have been determined in 3-D and have been used to demonstrate the sample studied has undergone a complex deformation history. The mean axes of curvature of inclusion trails (FIA) in cores and rims of garnet porphyroblasts on both limbs of the fold are oblique to the macroscopic fold axis, do not change bulk asymmetry across the fold, and are thus not related to the macroscopic fold. This indicates that garnet growth occurred early in the deformation history and pre-dates this folding.
- (2) A change in plunge of the garnet core–rim FIA across the fold is observed. The mean orientations of

inclusion trail surfaces in the cores and rims of garnet porphyroblasts adjacent quartz-rich layers (Grt_{aq} and Grt_{qs}) of the same generation on each limb define a tighter apparent fold than in the idioblastic garnet in mica-rich layers (Grt_{p}). It is unclear whether or not this open apparent fold existed before garnet core growth. This uncertainty in this part of the deformation history means that the inclusion trail geometry can be explained by interpretations involving either rotation or non-rotation of the porphyroblasts after their growth. However, the orientation of the apparent fold axis in Grt_{p} is within 32° of the macroscopic fold axis, compared to within 17° for the tabular porphyroblasts. This is more easily explained by an interpretation that involves rotation of the porphyroblasts during folding, than one involving no porphyroblast rotation.

(3) If a rotation interpretation is correct, porphyroblasts adjacent to quartz-rich layers have rotated more than those hosted completely in mica-rich layers. The reason for this appears to be due to more effective deformation partitioning around porphyroblasts in mica-rich layers where a crenulation cleavage is well developed. Deformation was unable to partition effectively around porphyroblasts adjacent to quartz-rich layers due to these layers being mechanically stronger, and consequently these porphyroblasts have spun with the fold limbs, but to a lesser degree than the limbs.

(4) If an interpretation involving no porphyroblast rotation is invoked then a gentle pre-porphyroblast fold must be inferred to explain the observed inclusion trail geometry.

ACKNOWLEDGEMENTS

I thank T. Bell for his boundless enthusiasm, supervisory support, and for critical assessments of early versions of this manuscript. K. Hickey, R. Newman, and A. Boyle are thanked for their useful discussions on subjects contained within this paper. I acknowledge the support of an International Postgraduate Scholarship during my PhD at James Cook University, Australia.

REFERENCES

- Bell, T. H., 1981. Foliation development: the contribution, geometry and significance of progressive bulk inhomogeneous shortening. *Tectonophysics*, **75**, 273–296.
- Bell, T. H., 1985. Deformation partitioning and porphyroblast rotation in metamorphic rocks: a radical reinterpretation. *Journal of Metamorphic Geology*, **3**, 109–118.
- Bell, T. H. & Chen, A., 2002. The development of spiral-shaped inclusion trails during multiple metamorphism and folding. *Journal of Metamorphic Geology*, **20**, 397–412.
- Bell, T. H. & Forde, A., 1995. On the significance of foliation patterns preserved around folds by mineral overgrowth. *Tectonophysics*, **246**, 171–181.
- Bell, T. H., Forde, A. & Wang, J., 1995. A new indicator of movement direction during orogenesis: measurement technique and application to the Alps. *Terra Nova*, **7**, 500–508.
- Bell, T. H. & Hayward, N., 1991. Episodic metamorphic reactions during orogenesis: the control of deformation partitioning on reaction sites and reaction duration. *Journal of Metamorphic Geology*, **9**, 619–640.
- Bell, T. H. & Hickey, K. A., 1997. Distribution of pre-folding linear indicators of movement direction around the Spring Hill Synform, Vermont; significance for mechanism of folding in this portion of the Appalachians. *Tectonophysics*, **274**, 274–294.
- Bell, T. H., Hickey, K. A. & Wang, J., 1997. Spiral and staircase inclusion trail axes within garnet and staurolite porphyroblasts from the schists of the Bolton Syncline, Connecticut: timing of porphyroblast growth and effects of fold development. *Journal of Metamorphic Geology*, **15**, 467–478.
- Bell, T. H. & Johnson, S. E., 1992. Shear sense: a new approach that resolves conflict between criteria in metamorphic rocks. *Journal of Metamorphic Geology*, **10**, 99–124.
- Bell, T. H., Johnson, S. E., Davis, B., Forde, A., Hayward, N. & Wilkins, C., 1992. Porphyroblast inclusion trail orientation data: eppure non son girate! *Journal of Metamorphic Geology*, **10**, 295–307.
- Bell, T. H., Rubenach, M. J. & Flemming, P. D., 1986. Porphyroblast nucleation, growth and dissolution in regional metamorphic rocks as a function of deformation partitioning during foliation development. *Journal of Metamorphic Geology*, **4**, 37–67.
- Billings, M. P., 1935. Geology of the Littleton and Moosilauke quadrangles, New Hampshire. *Geological Society of America Monograph*.
- Billings, M. P., 1937. Regional Metamorphism of the Littleton-Moosilauke area, New Hampshire. *Geological Society of America Bulletin*, **48**, 463–566.
- Bradley, D. C., 1983. Tectonics of the Acadian Orogeny in New England and adjacent Canada. *Journal of Geology*, **91**, 381–400.
- Busa, M. & Gray, N., 1992. Rotated staurolite porphyroblasts in the Littleton Schist at Bolton, Connecticut, USA. *Journal of Metamorphic Geology*, **10**, 627–636.
- De Bremaeker, J. C. & Brecker, E. B., 1978. Finite element models of folding. *Tectonophysics*, **50**, 349–367.
- Florence, F. P., Spear, F. S. & Kohn, M. J., 1993. P-T paths from northwestern New Hampshire: metamorphic evidence for stacking in a thrust/nappe complex. *American Journal of Science*, **293**, 939–979.
- Forde, A. & Bell, T. H., 1993. The rotation of garnet porphyroblasts around a single fold, Lukmanier Pass, Central Alps. Discussion. *Journal of Structural Geology*, **15**, 1365–1368.
- Ghosh, S. K. & Ramberg, H., 1976. Reorientation of inclusions by combination of pure shear and simple shear. *Tectonophysics*, **34**, 1–70.
- Hickey, K. A. & Bell, T. H., 1999. Behaviour of rigid objects during deformation and metamorphism; a test using schists from the Bolton Syncline, Connecticut, USA. *Journal of Metamorphic Geology*, **17**, 210–228.
- Hickey, K. A. & Bell, T. H., 2001. Resolving complexities associated with the timing of macroscopic folds in multiply deformed terrains The Spring Hill Synform, Vermont. *Bulletin of the Geological Society of America*, **113**, 1282–1298.
- Jeffrey, G. B., 1922. The motion of ellipsoidal particles immersed in a viscous fluid. *Royal Society of London Proceedings A.*, **102**, 161–179.
- Jiang, D., 2001. Reading history of folding from porphyroblasts. *Journal of Structural Geology*, **23**, 1327–1335.
- Jezek, J., Melka, R., Schulmann, K. & Venera, Z., 1994. The behaviour of rigid triaxial ellipsoidal particles in viscous flows – modeling of fabric evolution in a multiparticle system. *Tectonophysics*, **229**, 165–180.
- Kraus, J. & Williams, P. F., 2001. A new spin on 'non-rotating' porphyroblasts: implications of cleavage refraction and reference frames. *Journal of Structural Geology*, **23**, 963–971.
- Mancktelow, N. S., 1992. StereoplotXL. (*Stereographic projection software for Mac OS8*).

- Mancktelow, N. S. & Visser, P., 1993. The rotation of garnet porphyroblasts around a single fold, Lukmanier Pass, Central Alps. *Reply. Journal of Structural Geology*, **15**, 11, 1369–1372.
- Means, W. D., Hobbs, B. E., Lister, G. S. & Williams, P. F., 1980. Vorticity and non-coaxiality in progressive deformation. *Journal of Structural Geology*, **2**, 371–378.
- Passchier, C. W. & Trouw, R. A. J., 1996. *Microtectonics*. Springer Verlag, New York.
- Passchier, C. W., Trouw, R. A. J., Zwart, H. J. & Vissers, R. L. M., 1992. Porphyroblast rotation: Eppur si muove? *Journal of Metamorphic Geology*, **10**, 283–294.
- Pennachioni, G., Di Toro, G. & Mancktelow, N. S., 2001. Strain-insensitive preferred orientation of porphyroclasts in Monte Mary mylonite. *Journal of Structural Geology*, **23**, 1281–1298.
- Piazolo, S., Bons, P. D. & Passchier, C. W., 2002. The influence of matrix rheology and vorticity on fabric development of populations of rigid objects during plane strain deformation. *Tectonophysics*, **351**, 315–329.
- Ramberg, H., 1964. Selective buckling of composite layers with contrasting rheological properties, a theory for simultaneous formation of several order folds. *Tectonophysics*, **1**, 307–341.
- Ramsay, J. G., 1967. *Folding and Fracturing of Rocks*. McGraw-Hill, New York.
- Rumble, D., 1969. Stratigraphic, structural and petrologic studies in the Mt. Cube area, New Hampshire-Vermont. *PhD Thesis, Harvard University, Cambridge, MA, USA*.
- Spear, F. S. & Daniel, C. G., 2001. Diffusion control of garnet growth. Harpswell Neck, Maine, USA. *Journal of Metamorphic Geology*, **19**, 179–195.
- Spear, F. S. & Rumble, D., 1986. Pressure, temperature and structural evolution of the Orfordville belt, west central New Hampshire. *Journal of Petrology*, **27**, 1071–1093.
- Spiess, R. & Bell, T. H., 1996. Microstructural controls on sites of metamorphic reaction: a case study of the inter-relationship between deformation and metamorphism. *European Journal of Mineralogy*, **8**, 165–186.
- Stallard, A. R., 1999. Porphyroblast-matrix microstructures and garnet compositional zoning: constraints on foliation development, fold mechanisms and porphyroblast growth. *PhD Thesis, James Cook University, Townsville, QLD, Australia*.
- Stallard, A. R. & Hickey, K. H., 2001. Fold mechanisms in the Canton Schist: constraints on the contribution of flexural flow. *Journal of Structural Geology*, **23**, 1865–1881.
- Sutter, J. F., Ratcliffe, N. M. & Musaka, S. B., 1985. $^{40}\text{Ar}/^{39}\text{Ar}$ and K-Ar data bearing on the metamorphic and tectonic history of western New England. *Geological Society of America Bulletin*, **96**, 123–136.
- Timms, N. E., 2002. A tectonic evolution through microstructures: Orford to Piermont area of the New England Appalachians, west-central New Hampshire, USA. *PhD Thesis, James Cook University, Townsville, QLD, Australia*.
- Vissers, P. & Mancktelow, N. S., 1992. The rotation of garnet porphyroblasts around a single fold. *Lukmanier Pass, Central Alps. Journal of Structural Geology*, **11**, 231–244.
- Williams, M. L., 1994. Sigmoidal inclusion trails, punctuated fabric development, and interactions between metamorphism and deformation. *Journal of Metamorphic Geology*, **12**, 1–21.
- Williams, P. F. & Jiang, D., 1999. Rotating Garnets. *Journal of Metamorphic Geology*, **17**, 367–378.
- Williams, P. F. & Schoneveld, C. H. R., 1981. Garnet rotation and the development of axial plane crenulation cleavage. *Tectonophysics*, **78**, 307–334.

Received 18 March 2003; revision accepted 20 August 2003.